Journal of Materials & Environmental Sustainability Research (2022), 2(3): 12-36
p-ISSN: 2811-1338; e-ISSN: 2811-132X
DOI: https://doi.org/10.55455/jmesr.2022.007

Original Research Paper

Adsorption of organic dyes by carbonized and chemically activated *Cassia fistula* pods

Alimoh H. Alabi [1]*, Muhammed M. Hashirudeen [1], Reuben K. Olaleye [1], Ebenezer O. Oladele [2]

[1] Department of Chemistry, Faculty of Science, University of Ibadan, Ibadan, Nigeria
[2] Department of Chemistry, Faculty of Science, Joseph Ayo Babalola University, Ondo, Nigeria
*Corresponding author: Alimoh H. Alabi (helenalabie3@yahoo.com)

Received: June 21, 2022; Revised: September 8, 2022; Accepted: September 11, 2022; Published: September 19, 2022

Handling Editor: Nnanake-Abasi O. Offiong

Abstract:
The kinetics and mechanism of methylene blue and Congo red adsorption by carbonized and chemical activated *Cassia fistula* was investigated for various physicochemical parameters in a batch system. The adsorbents were characterized using Fourier Transform Infrared Spectroscopy (FTIR), Scanning Electron Microscope (SEM), and Energy Dispersive X-Ray (EDX). The results showed that the adsorbents were rich in carbon content and heterogeneous large surface area for organic dye interaction. To understand the adsorption process, the equilibrium data was tested using Langmuir, Freundlich, Temkin and Brunauer-Emmett-Teller (BET) adsorption isotherms. The good physisorption adsorption process is indicated by the Freundlich constant, n>1. Furthermore, -0.0188, 0.0007, and 0.6990 for methylene blue; -0.0692, 0.0001 and 0.3856 for Congo red were obtained for ΔG^0, ΔH^0 and ΔS^0 thermodynamics parameters, respectively. Results from BET study revealed efficient dye adsorption and chemical activation of the adsorbent with hydrogen peroxide and potassium hydroxide. The regression coefficient (R^2) of carbonized and chemical activated *Cassia fistula* biomass were: 0.918, 0.742, and 0.878, for methylene blue; 0.708, 0.666 and 0.527 for Congo red at 60 °C. Results from adsorption studies proved that chemical-activated adsorbent from *Cassia fistula* pods is a promising effective and eco-friendly alternative for the removal of organic dyes from the aqueous system.

Keywords: Adsorption; *Cassia fistula*; Congo red; methylene blue; isotherms

DOI: 10.55455/jmesr.2022.007

1. Introduction

Numerous chemicals and substances are utilized to improve the quality of human daily life and consumer items due to advancements in science and technology. On the other hand, abuse and unregulated discharge of such substances into water bodies, on the other hand, frequently have long-term adverse consequences on aquatic life and human health. Most industrial pollutants are metal ions or recalcitrant organic chemicals, which persist in water bodies, aggravates the situation. These pollutants make river water unfit for drinking and recreational purposes (Schweiter & Noblet, 2018).

Irrigation and food production account for 70% of current global freshwater consumption, according to reports and statistics from several international organizations, this consumption is expected to rise by 19% (including rain-fed and irrigated agriculture) over the next 40 years as the world's population grows (UN Water, 2017). Water stress, in which available freshwater sources fail to satisfy demand due to low quality (a result of water pollution), is expected to affect two-thirds of the world's population by 2025 if no efforts to reduce water pollution are taken (UNESCO, 2017). Urbanization is the primary source of water contamination in developed countries. In developing countries, on the other hand, 70% of garbage is dumped into rivers, lakes, and coastal zones without being treated, and 90% of wastewater is released into rivers, lakes, and coastal zones (UN Water, 2017;

UNESCO, 2017). Dye pollution in industrial effluent and agricultural operations is a major concern due to its toxicity, bioaccumulation, biomagnifications, global range, and environmental persistence (Afonze & Sen, 2018).

When dyes are discharged into waste streams, they are colored and ionized aromatic organic molecules with complicated persistent molecular structures (Afroze & Sen, 2018). Industries such as textiles (Sokolowska-Gajda et al. 1996; Carmen & Daniela 2012), paper and pulp manufacturing (Carmen & Daniela, 2012), agriculture (Kross et al., 1996; Cook & Linden, 1997), food technology (Bhat & Mathur, 1998), light-harvesting arrays (Bensalah et al., 2009), photo-electrochemical cells (Wróbel et al., 2001), pharmaceutical (Carmen & Daniela 2012), tannery (Kabdaşli et al. 1999; Tünay et al. 1999), Kraft bleaching industries (Carmen & Daniela, 2012), etc. introduce a wide variety of organic dyes into the natural water resources or wastewater treatment systems (Afroze et al. 2015). Textile industries utilize the most water (up to 150 L of water to dye 1 kg of cotton) and are considered high dye polluters because only 2% of dyes produced are discharged directly into aqueous effluents (Jadhav et al. 2010; Crini, 2006). According to additional research, roughly 12% of synthetic dyes are wasted during production and processing operations, with approximately 20% of these dyes ending up in industrial wastewater (Demirbas, 2009).

Bioaccumulation and biomagnification are two major processes that endanger marine ecology and human life. Bioaccumulation occurs when a chemical's adsorption rate into an organism surpasses its metabolism and excretion rate (Wong, 2018). Contaminated producers are consumed by predators, increasing chemical concentrations further down the food chain. The pattern repeatedly continues, with biomagnification occurring as animals at higher levels in the food chain accumulate more chemicals (Matulik et al., 2017; Zenker et al., 2014). The compound must be long-lived, mobile, soluble in lipids, and biologically active for bioaccumulation and biomagnification to occur and induce detrimental effects in animals and humans (Peng et al., 2017). Toxins in a mother's body can be passed on to the fetus and babies through breast milk during pregnancy (Polanco Rodriguez et al., 2017). Such exposure is thought to affect child development (Tatsuta et al., 2017) and may result in irreversible brain damage, including autism spectrum disorders (Ye et al., 2017).

As a result, if left untreated, this ionic dye (methylene blue) can cause irreversible harm to the natural environment and human health. These toxic effluents pose a severe threat to the surrounding ecosystem (Afonze & Sen, 2018). The importance of preserving freshwater ecosystem has led to the development of a variety of techniques to purify wastewater of pollutants before discharge into rivers, including adsorption (Sohaimi et al., 2017; Wong et al., 2017), membrane filtration (Dickhout et al., 2017), electrochemical advanced oxidation methods (Moreira et al., 2017), (coagulation, membrane separation, foam flotation, precipitation, ozonation, ion exchange, filtration, solvent extraction, electrolysis, and liquid-liquid extraction (Afonze & Sen, 2018).

Activated carbon is the most widely used adsorbent due to its capacity for the adsorption of organic materials. This adsorbent is difficult to regenerate due to its high cost. In this context, the use of activated and chemically activated *Cassia fistula* as adsorbent is of great interest as a result of improved efficiency, easy accessibility and availability, cost-effectiveness, and waste recycling for sustainable development; thus, providing alternative effective and efficient adsorbent at low cost and proper waste management of the agricultural wastes. Only a few studies (Sen et al, 2011; Salleh et al, 2011) have been published on the carbonized and chemically activated *Cassia fistula* in the removal of ionic dyes.

Cassia fistula is a tropical deciduous tree that can reach a height of 20 m and a width of 3-5 m when fully grown. It contains high amount of ionizable groups such as C=O, –OH, C–H, C–C, C=C (Imran et al., 2019). It is a member of the Fabaceae legume family that grows in tropical areas such as India, Sri Lanka, Myanmar, and Nigeria. A shower of golden-yellow blossoms cascades from the tree's branches. When ripe, the fruits are cylindrical and highly elongated, turning brown but not splitting. The leaflets of *Cassia fistula* are paripinnate, oval, large, and oppositely placed.

This study analyses the mechanism of adsorption and kinetics of methylene blue and Congo red by *Cassia fistula*, as well as the various physicochemical factors that influence the rate of adsorption capacity. Methylene blue and Congo red adsorption have been studied in relation to initial solution pH, initial dye concentration, adsorbent dose, and temperature.

2. Materials and Methods

2.1 Adsorbent

Cassia fistula pods (golden shower) were collected from the Botanical Garden, University of Ibadan, washed with distilled water to remove adhering contaminants from the surface, crushed, and the seed extracted. Then it was air-dried before being dried in the oven at 105 ℃ for 60 min. The dried material was pulverized using an S. S. Pulwariser machine and sieved with a Tyler sieve to discrete sizes of 0.15 – 0.3 mm before being carbonized at 700 °C in an electrical muffle furnace under purified nitrogen (99.99%) flow and labeled unactivated carbonized *Cassia fistula* pod (CCF).

2.2 Chemical activation of the adsorbent

The process for chemical activation of the adsorbent with hydrogen peroxide (H_2O_2) was patterned after that described by Yingwen et al. (2012) and Liu (2019).

Exactly, 100 g of the carbonized *Cassia fistula* was impregnated with a 1:2 solution of hydrogen peroxide (w/v) and potassium hydroxide (w/v) separately in a mechanical shaker at room temperature. The samples were then activated in an electrical muffle furnace for 2 hours at 700 °C under pure nitrogen (99.99%) flow.

The activated samples were then washed with deionized water and 0.1 M hydrochloric acid until the neutral pH was achieved. The sample was pieces and then dried at 105 °C in an oven for 60 min, cooled in a desiccator, and collected in an airtight plastic container for analysis and adsorption studies. Chemically activated carbons produced from H_2O_2 and KOH activation were designated as HACF and PACF, respectively. The activated sample was then washed with deionized water and 0.1 M hydrochloric acid until neutral pH was achieved. The pieces were then dried at 105 °C in an oven for 60 min, cooled in a desiccator, and collected in an airtight plastic container for characterization analysis and adsorption studies.

The functional group on *Cassia fistula* biomass powder was determined using the PerkinElmer Spectrum Two, BX11 spectrometer. A scanning electron microscope–energy dispersive x-ray (Phenom ProX, Netherlands) was used to determine the surface morphology before adsorption. The surface area was determined using Brunauer-Emmett-Teller (BET) (Quantachrome NovaWin version 11.03, USA).

2.3 Adsorbate and other Chemicals

All chemicals used were of analytical grade. Methylene blue (MB), the typical basic cationic dye and Congo red (CR), an anionic dye were selected as the present study's adsorbate. Methylene blue and Congo red have the formulae: $C_{16}H_{18}ClN_3S \bullet 3H_2O$ and $C_{32}H_{22}N_6Na_2O_6S_2$, respectively, which were supplied by Sigma-Aldrich Pty. Ltd., Australia. It was used without further purification. The required amount of MB and CR (1,000 mg) was dissolved in deionized water and the solution was made up to mark in a 1-litre standard flask. This gives 1,000 mg/l (1,000 ppm) standard solutions. The pH of the solutions was changed by adding 0.1 M HCl or 0.1 M NaOH solutions, as necessary. All sample bottles and glassware were cleaned, rinsed with deionized water, and dried in the oven at 60 °C for 60 min. The visible spectrophotometer 721 (Baoshishan, Japan) was used to determine the amounts of methylene blue and Congo red dye in the solution. A Jenway 3520 pH meter was used to measure the pH of the solution. By removing samples at specified time intervals, the concentration of residual dye was quantified using a uv-visible spectrometer at a maximum wavelength corresponding to the maximum adsorption for the dye solution (λmax = 663 nm for MB and 497 nm for CR), centrifuged, and the supernatant was analyzed for residual MB and CR. A calibration curve was plotted between the dye solution's absorbance and concentration to create an absorbance–concentration profile.

2.4 Batch equilibrium and kinetic studies

Batch experiments using 50 mL of aqueous methylene blue and Congo red solutions of known concentration in a series of 250 mL conical flasks were used to determine adsorption studies with a known amount of adsorbent (0.20 g). The mixture was stirred thoroughly at a constant temperature using Labnet Orbit 1900 Digital Shaker at 150 rpm with a required time at 15, 30, 60, 90, 120, 150, 180, and 240 min (300, 303, 313, 318, 323 and 333 K). The flasks were then removed from the shaker, and the final concentration of dye in the solution was determined

using a UV-vis spectrophotometer at maximum wavelengths of MB (663 nm) and CR (497 nm) (Baoshishan 721 Visible Spectrophotometer, Japan). The following equation (Equation 1) was used to compute the amount of dye adsorption at equilibrium Q_e (mg/g) (Weber & Morris, 1963).

$$q_e = \frac{(Co - Ce)V}{M} \quad (1)$$

Kinetic experiments used the same technique as equilibrium tests. The dye concentrations in the water samples were also monitored at pre-determined intervals. At time (t), the amount of adsorption (Q_t) in mg/g is calculated from Equation 2 (Weber & Morris, 1963).

$$q_t = \frac{(Co - Ct)V}{M} \quad (2)$$

Dye removal efficiency, i.e., % of adsorption was calculated as:

$$\% \text{ Adsorption} = \frac{(Co - Ce)}{Co} \times 100 \quad (3)$$

Where C_0 represents the initial dye concentration (mL), C_t represents the dye concentration at time t, V represents the volume of solution (L), and m is the mass of *C. fistula* powder (g). In general, all measurements are consistent to within ±10%.

2.4.1 Effect of dosage

Volume 50 mL of the dyes MB and CR were agitated with different masses (0.2, 0.3, 0.4, 0.5, 0.6, 0.7, 0.8, 0.9, and 1.0g) of the adsorbents CCF, HACF, and PACF for 3 hours at 150 rpm. A uv-visible spectrophotometer was then used to quantify the concentration of unabsorbed dyes at room temperature.

2.4.2 Effect of initial concentration

Mass 0.20 g of CCF, HACF and PACF sample were added to each 50 mL of volume of MB and CR solution. The initial concentrations of dye solution tested were 20, 30, 40, 50, 60, 70, 80, 90 and 100 ppm (mg/L) and the experiments varied at 15, 30, 60, 90, 120, 150, 180, and 240 min at room temperature.

2.4.3 Effect of contact time

Mass 0.20 g sample CCF, HACF and PACF were added to each 50 mL volume of MB and CR solution. The experiments varied at room temperature at 15, 30, 60, 90, 120, 150, 180, and 240 min.

2.4.4 Effect of temperature

At varying initial concentrations, 0.20 g CCF, HACF, and PACF samples were added to each 100 mL of volume of MB and CR aqueous solution. The experiments were carried out at 300, 303, 313, 318, 323 and 333 K for 210 min.

2.5.5 Effect of solution pH

The solution's pH was investigated at pH 4, 6, 8, 10, and 12; 0.30 g of CCF, HACF, and PACF were added to each 50 mL of MB and CR aqueous solution with an initial concentration of 100 mg/L for a constant adsorption time of 210 min.

3. Results and Discussion

3.1 Characterization of prepared adsorbents

There are various analytical techniques used to detect the surface area, pore volume, and pore size of adsorbent material apart from the Brunauer-Emmett-Teller (BET). The Barrett-Joyner-Helenda (BJH) method, which is used to describe mesopores, Horvath-Kawazoe (HK) method which is generally applied to describe micropores and Density Functional Theory (DFT). BET is more accurate and reliable for calculating the specific surface area of

adsorbents as the ISO 9277 standard of calculating surface area of solids is based on this method (Gibson et al. 2020). Table 1 shows the surface area, pore volume and pore size of PACF, HACF and CCF.

Table 1: Comparison of surface area, pore volume, and pore size of PACF, HACF, and CCF using different methods

Methods	Surface area (m^2/g)		
	PACF	HACF	CCF
Single Point BET	2.498×10^2	2.349×10^2	1.363×10^2
Multiple Point BET	3.525×10^2	4.242×10^2	2.510×10^2
	Pore volume (cc/g)		
	PACF	HACF	CCF
BJH Pore Volume	2.166×10^{-1}	2.177×10^{-1}	1.267×10^{-1}
	Pore size (nm)		
	PACF	HACF	CCF
BJH Pore Diameter	2.132	2.105	2.100

The adsorption capacity of *C. fistula* biomass is determined by the biomass's porosity and the chemical reactivity of the functional groups on the surface. As a result, understanding surface functional groups can provide information on the biomass's adsorption capacity. Figure 1− 9 shows the FTIR spectra of the adsorbents CCF, HACF, and PACF before and after MB and CR adsorption.

The CCF spectra indicate the strong band signal of 3383.55 cm^{-1} for –OH. The medium adsorption bands of 2924.7 cm^{-1} and 2853 cm^{-1} are for the –C-H i.e., methyl and methylene. Also, the C≡C terminal alkyne (mono substituted) was indicated by 2116.65 cm^{-1}. 1582.24 cm^{-1} and1431.40 cm^{-1} represents the carbonyl group. Lower bands of 874.38 cm^{-1}, 807.42 cm^{-1}, and 746.84 cm^{-1} are attributed to the CH_{deform} (out plane).

In HACF, seven strong signals of the –OH functional group were seen ranging from 3554.7 cm^{-1} to 3775.72 cm^{-1}. This includes the –OH signal bond and the –OH sharp for free and unbounded. The –CH bands of methyl and methylene were shifted to 2924.7 cm^{-1} and 2855cm^{-1}as a result of the activation with peroxide. There were also the disappearance of the C≡C band, one of the carbonyl peaks, and two –CH_{deform} bands, shifts of the other carbonyl group to 1619.36 cm^{-1} and the maintenance of a –CH_{deform} peak at 874.04 cm^{-1}.

PACF also demonstrated a similar strong –OH functional group for both the single bond and free and unbounded in the range of 3872.30 cm^{-1} – 3573 cm^{-1}. 2311.36 cm^{-1} band of C≡C was also observed followed by the 1560.15 cm^{-1} and 1213.37 cm^{-1} for the carbonyl group. The fingerprint region shows shifts in the three bands to 873.61 cm^{-1}, 813.48, cm^{-1} and 755.93 cm^{-1} for the CH_{deform}.

Following the adsorption of methylene blue on HACF, a new band for –OH was introduced at 3157.40 cm^{-1}; 1579 cm^{-1}, 1452.20 cm^{-1}, 1385.7 cm^{-1} and 1023.1 cm^{-1} for C=O and C-O respectively. The CH_{deform} bands were also presented at 1164 cm^{-1}, 1117.8 cm^{-1}, and 1060.3 cm^{-1}. In CCF, there were shifts of an –OH band to 3160.76cm^{-1} and the carbonyl bands to 1579 cm^{-1} and 1427.99 cm^{-1}. The disappearance of the –CH of methyl and methylene bands was also observed. Also, CH_{deform} bands were introduced at 1163 cm^{-1} and 1023 cm^{-1}. Similarly, in PACF, -OH band shifts were noticed at 3146.03 cm^{-1}, -C=O at 1564.5 cm^{-1} and 1422.6 cm^{-1} with an introduction of –CH_{deform} band at 1164.12 cm^{-1}.

For Congo red, there were also some shiftings, disappearance of peaks, and the appearance of new peaks. The CCF-dye-laden adsorbent has the –OH peak shifted to 3174.57 cm^{-1}, the carbonyl functional group of ether and carboxylic group shifted to 1579 cm^{-1} and 1433.6 $cm^{-1}$with the introduction of new peaks at1700.3 cm^{-1}, 1165.43 cm^{-1} and 1025.6 cm^{-1}. While six peaks indicating –OH disappeared after adsorption in HACF, there was a shift to 3160.88 $cm^{-1}$for –OH, the disappearance of the –CH of the methyl and methylene bands, shifting of the –CO group

to 1679 cm^{-1} alongside the appearance of new carbonyl functional group at 1565 cm^{-1}, 1431.21 cm^{-1}, 1162 cm^{-1} and 1022.4 cm^{-1}. PACF also recorded the disappearance of some –OH bands. Shift to 3854.5 cm^{-1}, 3750.6 cm^{-1} and 3020.89 cm^{-1} for the –OH groups and 1693.4 cm^{-1} and 1226.60 cm^{-1} for the carbonyl group.

The surface availability of adsorbents for the adsorption of toxins' molecules is determined using scanning electron microscopy (Adebayo et al., 2020). The surface characteristics of the particles are important in the attachment of contaminants to the adsorbent's surface. Surface homogeneity and heterogeneity affect the adsorbent's ability to remove the target pollutants (Imran at al., 2019). Energy Dispersive X-ray (EDX) analysis determines the elemental composition of an adsorbent.

Figures 10 – 12 show scanning electron microscopy (SEM) images of the adsorbents before adsorption. The PACF and HACF (Fig. 11 and 12) have heterogeneous morphologies, sizes, fissures, and roughness on the surface, which offered a vast surface area for MB and CR interaction and smoothed out when the adsorbents were connected to the surface. The EDX patterns shown in Figure 13-15 reveal that the biomass is rich in carbon content at 83.92% by weight. Other elements identified are O and Ca with varying degrees.

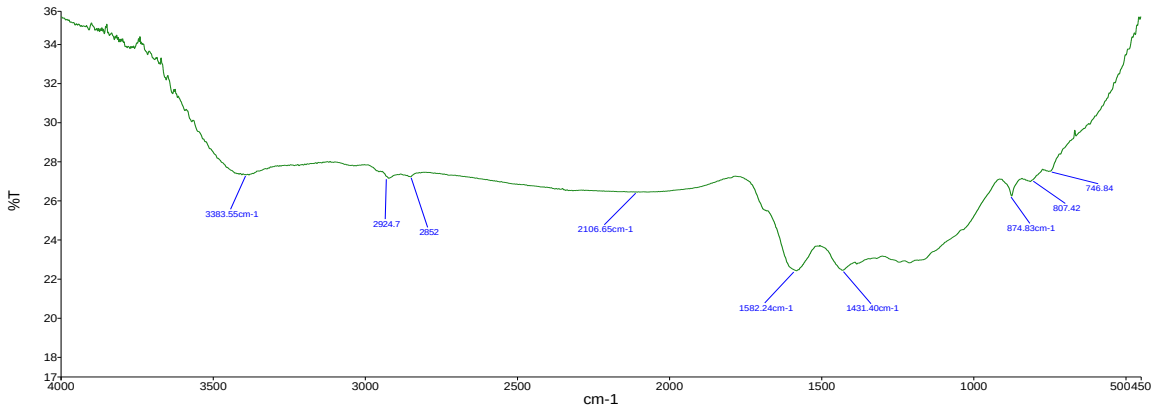

Figure 1: FTIR spectra of CCF (the y-axis (%T) represents the percent transmittance, while the x-axis corresponds to the wavenumber (in cm^{-1}))

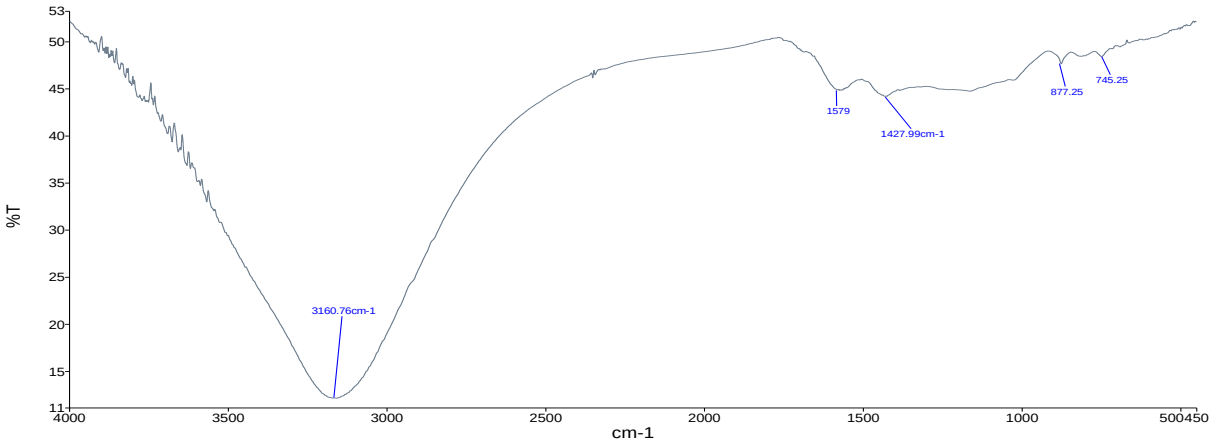

Figure 2: FTIR spectra of CCF loaded with MB (the y-axis (%T) represents the percent transmittance, while the x-axis corresponds to the wavenumber (in cm^{-1}))

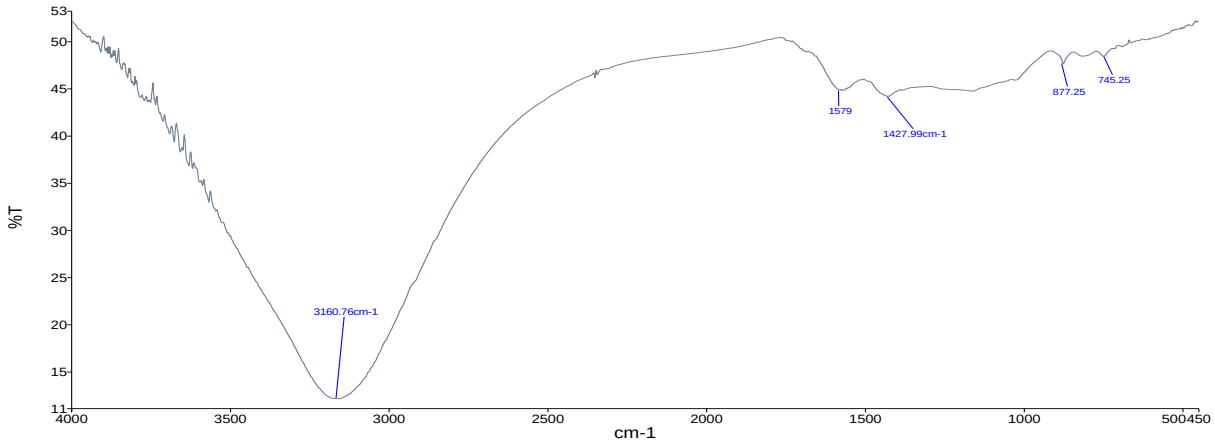

Figure 3: FTIR spectra of CCF loaded with CR (the y-axis (%T) represents the percent transmittance, while the x-axis corresponds to the wavenumber (in cm^{-1}))

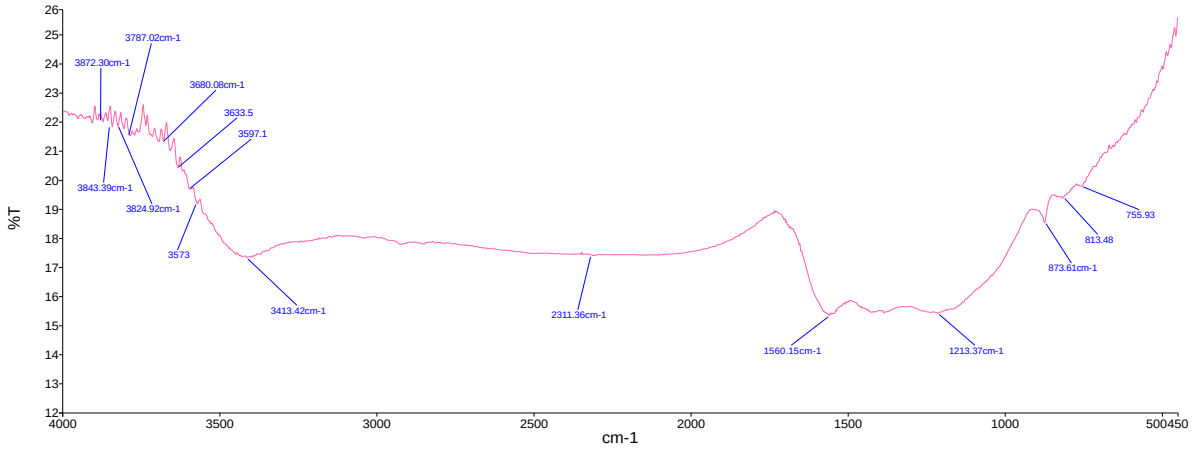

Figure 4: FTIR spectra of PACF (the y-axis (%T) represents the percent transmittance, while the x-axis corresponds to the wavenumber (in cm^{-1}))

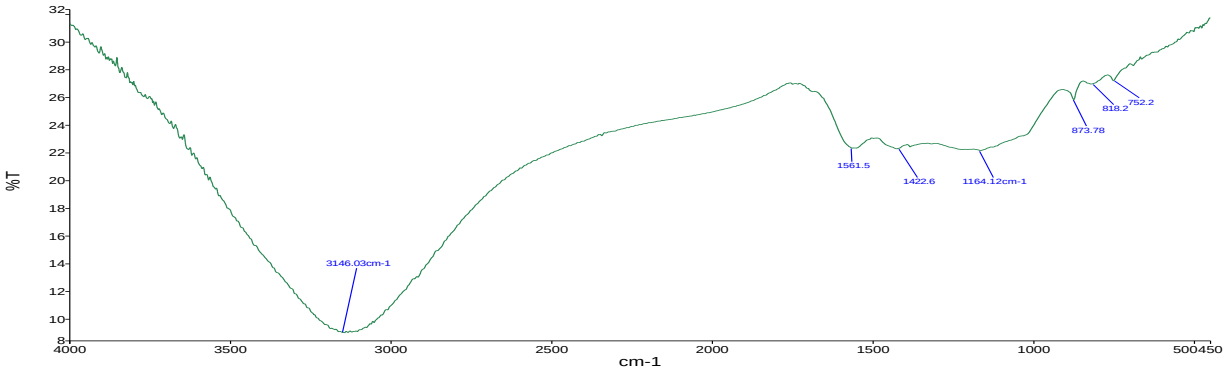

Figure 5: FTIR spectra of PACF loaded with MB (the y-axis (%T) represents the percent transmittance, while the x-axis corresponds to the wavenumber (in cm^{-1}))

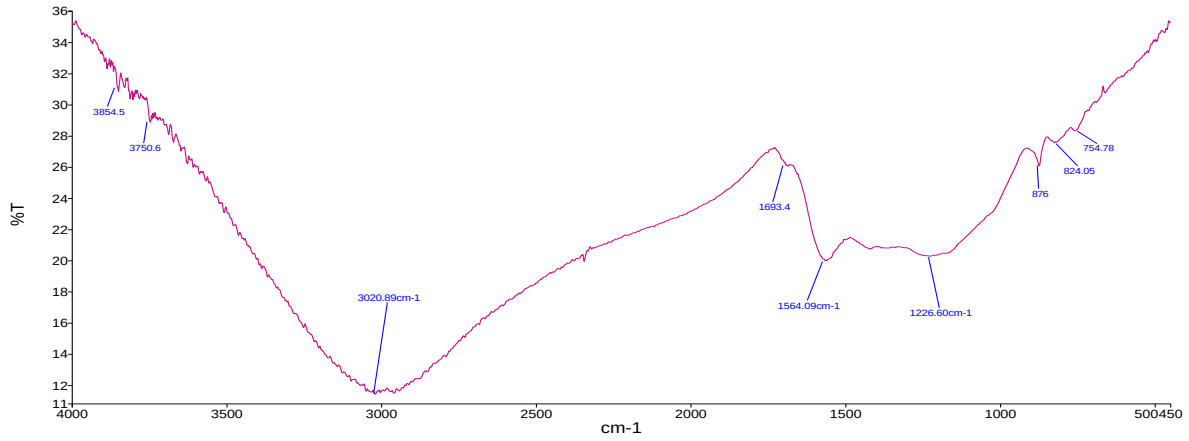

Figure 6: FTIR spectra of PACF loaded with CR (the y-axis (%T) represents the percent transmittance, while the x-axis corresponds to the wavenumber (in cm^{-1}))

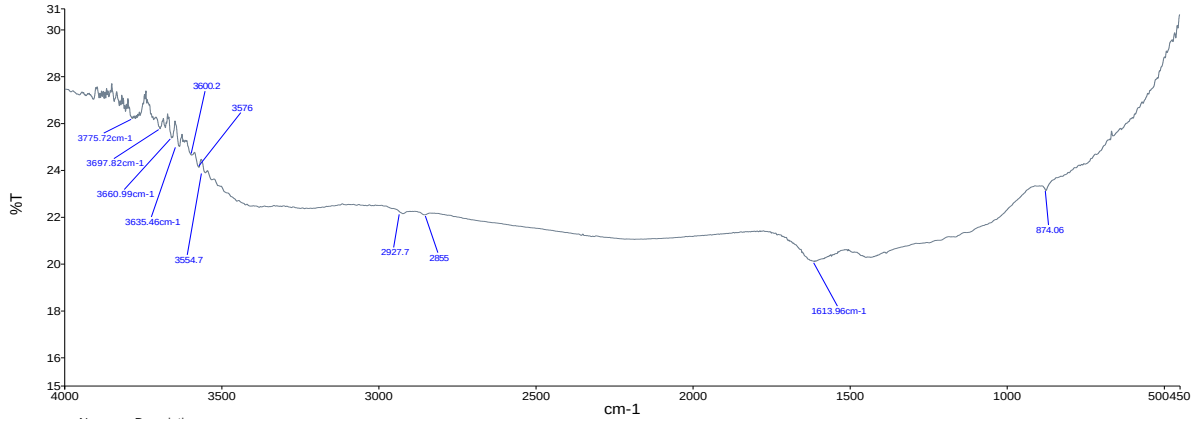

Figure 7: FTIR spectra of HACF (the y-axis (%T) represents the percent transmittance, while the x-axis corresponds to the wavenumber (in cm^{-1}))

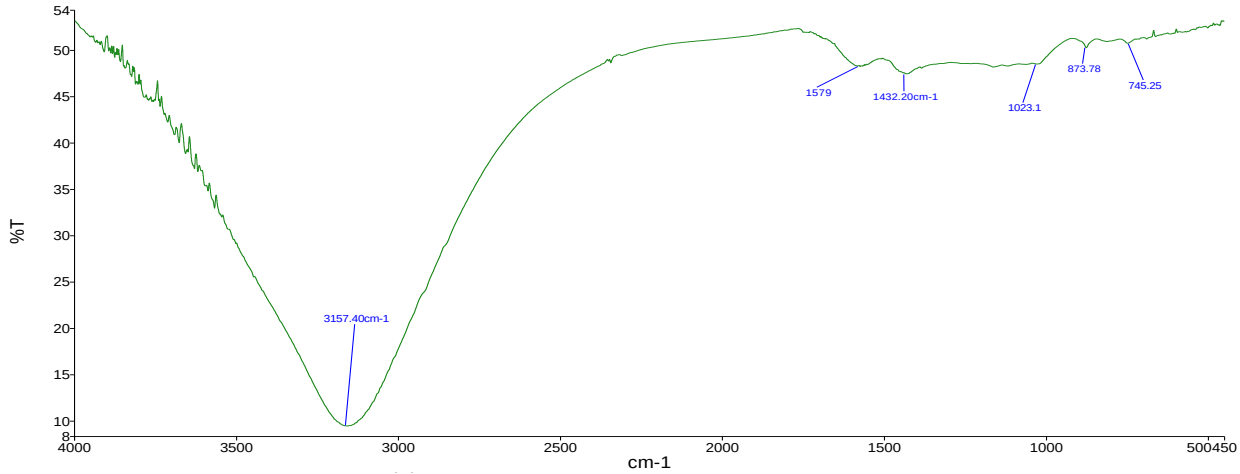

Figure 8: FTIR spectra of HACF loaded with MB (the y-axis (%T) represents the percent transmittance, while the x-axis corresponds to the wavenumber (in cm^{-1}))

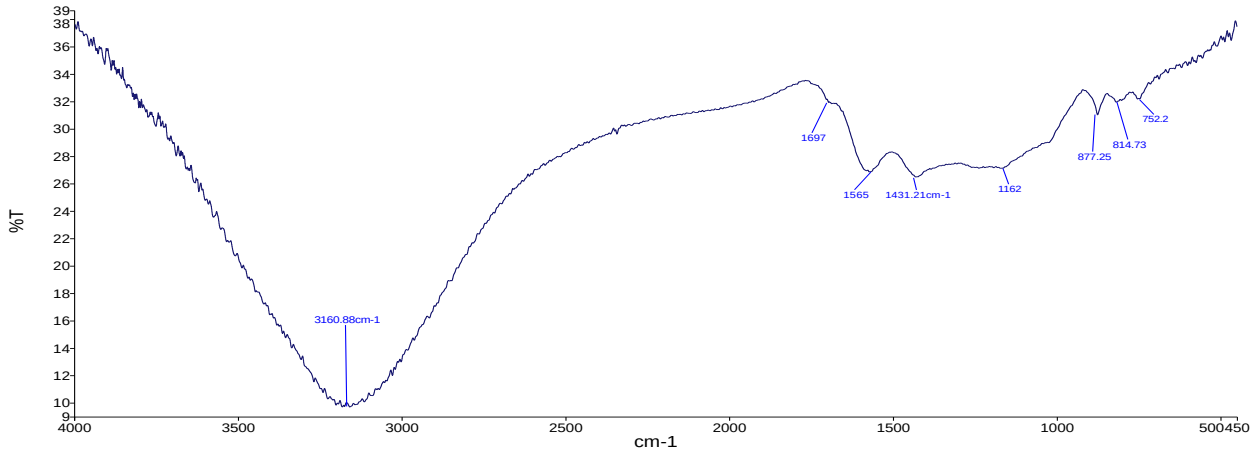

Figure 9: FTIR spectra of HACF loaded with CR (the y-axis (%T) represents the percent transmittance, while the x-axis corresponds to the wavenumber (in cm^{-1}))

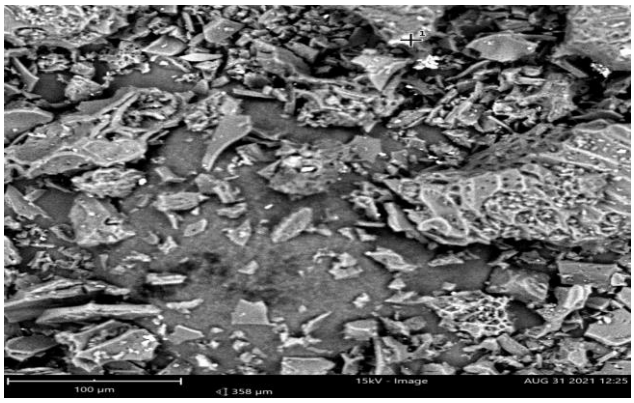

Figure 10: SEM image of PACF

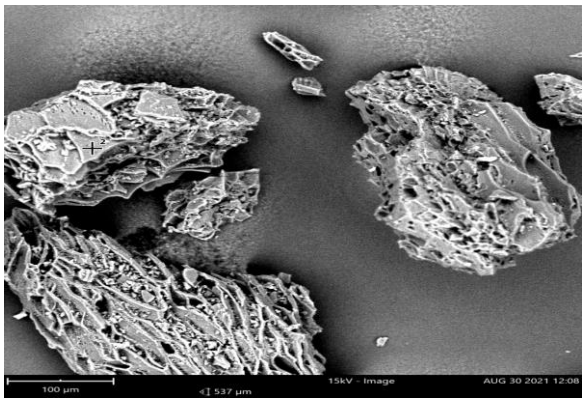

Figure 11: SEM image of HACF

Figure 12: SEM Image of CCF

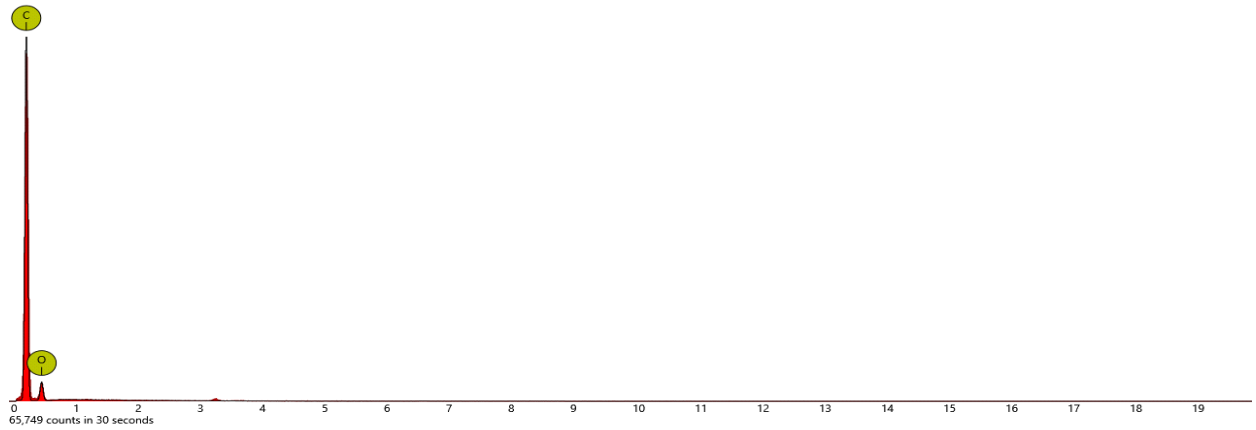

Figure 13: EDX elemental spectra of PACF (the y-axis represents counts, while the x-axis corresponds to energy (in KeV))

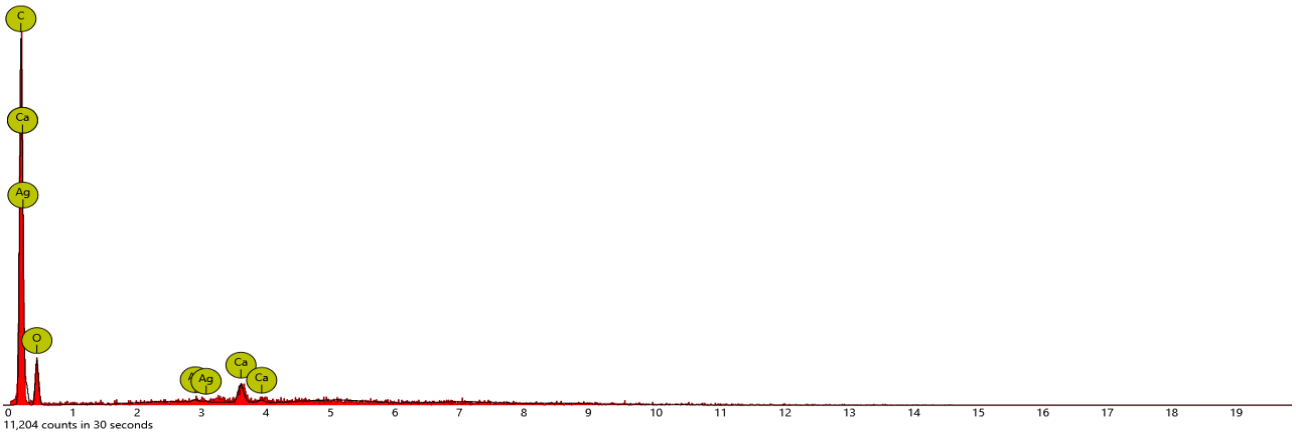

Figure 14: EDX elemental spectra of HACF (the y-axis represents counts, while the x-axis corresponds to energy (in KeV))

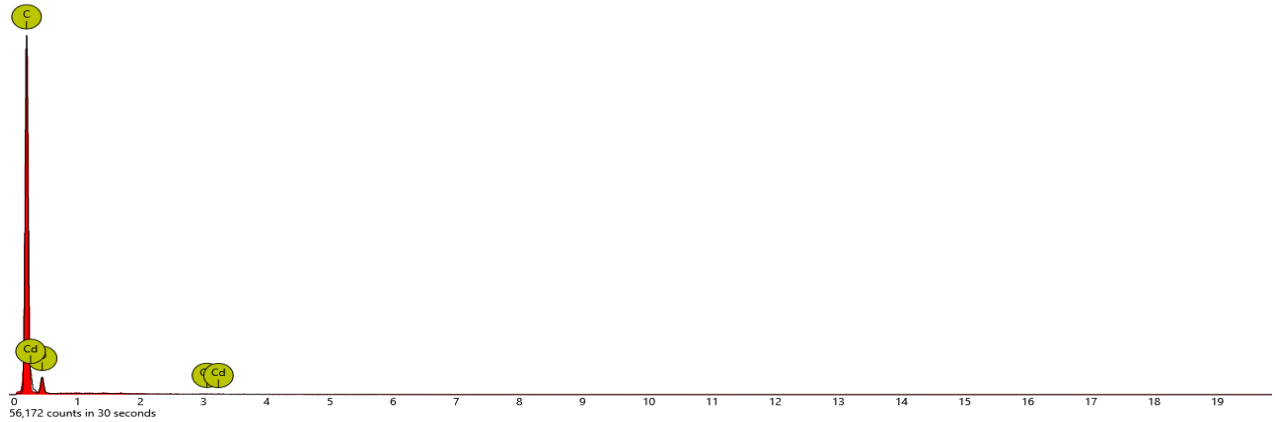

Figure 15: EDX elemental spectra of CCF (the y-axis represents counts, while the x-axis corresponds to energy (in KeV))

The pH of the solution measures the molar concentration of hydrogen ions in a solution. Solution pH < 7 is acidic while solution pH >7 is basic. A change in the solution pH due to changes in adsorbent surface properties and dye chemistry is a critical parameter for solute adsorption. The pH at which the surface charges and electrical charge density on a surface are zero is known as the point of zero charges (pzc), and it is widely used to define the electrokinetic properties of a surface.

It can be deduced from Figure 16 that the surface charge of the adsorbents becomes negatively charged at pH greater than the pH_{pzc} of the adsorbents and positively charged at pH lower than the pH_{pzc} (Srivastava & Sillanpaa, 2017).

In contrast to the adsorbent pH 8.81 and pH_{phz} 8.80 of CCF, a comparison of the pH of the adsorbent pH 8.24 for PACF and pH 8.42 for HACF indicates considerable surface modification of the adsorbent pH_{phz}. Table 2 summarizes pH and point of zero charge (pH_{pzc}) of *C. fistula* and its modified biomass products.

Table 2. pH and point of zero charge (pHpzc) of the adsorbents

Adsorbents	pH	pH_{pzc}
Potassium hydroxide Activated *Cassia fistula* (PACF)	8.24	9.00
Hydrogen peroxide Activated *Cassia fistula* (HACF)	8.42	8.30
Carbonized *Cassia fistula* pod (CCF)	8.81	8.80

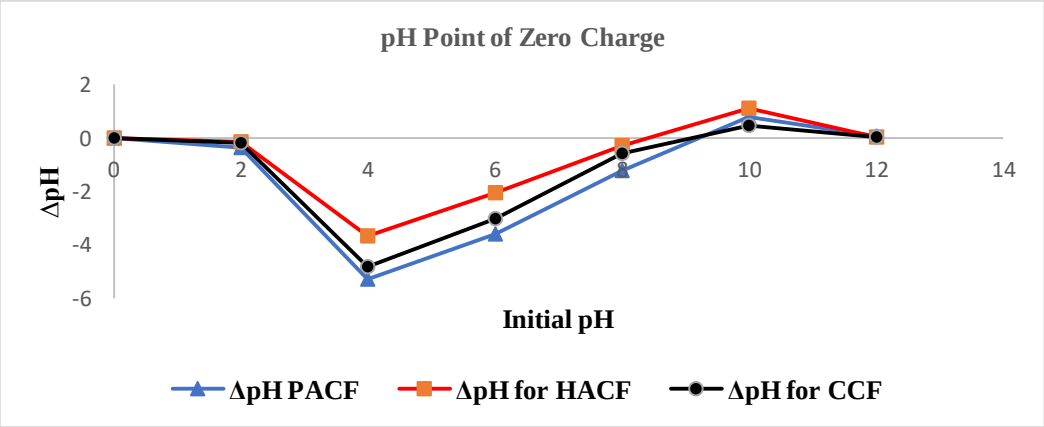

Figure 16: Plot of final pH against initial pH of pHpzc PACF, HACF and CCF

3.2 Effects of operating parameters

3.2.1 Effect of adsorbent dosage

Adsorbent dosage is a crucial process parameter that describes an adsorbent's ability to absorb a specific amount of adsorbent under any operating condition (Sari et al., 2007). The effect of adsorbent dosage gives an understanding of an adsorbent's effectiveness and the capacity of a dye to be adsorbed at a low-cost minimal dose (Salleh et al., 2011). The maximum removal for Congo red and methylene blue onto PACF, HACF and CCF was seen at 0.2 g respectively, as shown in Figure 17, after which the removal effectiveness dropped. Due to over-saturation and high mobility in the sorption medium, the number of binding sites available for CR and MB on the adsorbent decreases.

Oladele et al. (2019) studied the influence of adsorbent dose on methylene blue dye removal by *C. fistula*, finding that when the adsorbent dose was decreased, the percentage of dye removal increased. According to Yagub et al. (2014), the amount of adsorbent used in the removal methylene blue pollution by natural and modified low-cost agricultural by-products increased the amount of methylene blue dye adsorption. Feng et al. (2012) studied the impacts of adsorbent dose on methylene blue removal by Swede rape straw. They discovered that the percentage of dye removal increased as the adsorbent dose was reduced.

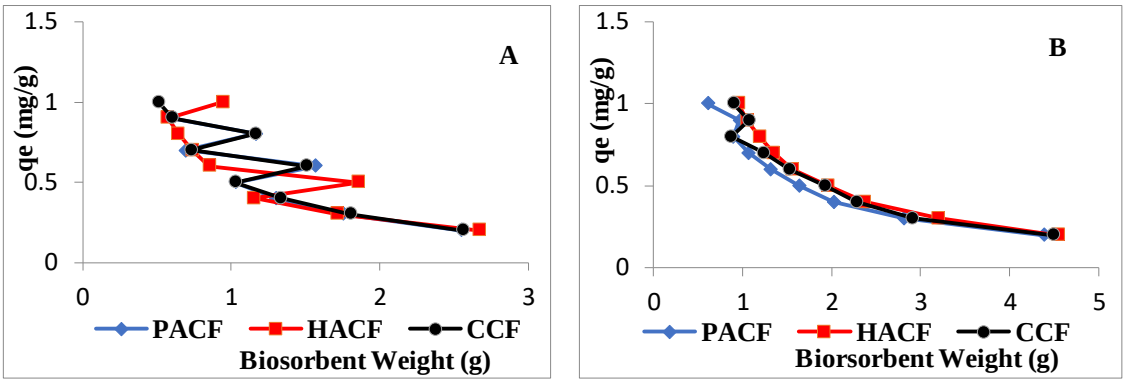

Figure 17: The effect of adsorbent (PACF, HACF and CCF) dosage on (A) methylene blue and (B) Congo red (20 ppm) adsorption. (Volume of dye: 50 mL; temperature 27 °C; agitation speed: 150 rpm)

3.2.2 Effect of Contact Time

Methylene blue (MB) adsorption onto CCF, PACF, and HACF needed 240 minutes with continuous agitation for the adsorbents to remove the highest percentage (83.21%, 83.30% and 4.42% removal) and optimal removal (21.80, 20.81 and 21.04 mg/g) of the dyes from the solution. However, for optimum removal of Congo red (CR) onto CCF with 69.73% removal (17.43 mg/g), 120 min were needed, whereas for PACF with 69.92% (17.48 mg/g), 30 min were required. With a 68.52% percent (17.13 mg/g) removal rate, HACF takes 240 min to remove CR from the solution. The speed of sorption may be attributable to the occupation of high-affinity binding sites. The relative inaccessibility of the remaining binding sites may be indicated by slow kinetics beyond that time. Figure 18 depicts the adsorption of CR and MB on CCF, PACF, and HACF.

According to numerous experiments, the quantity of dye adsorption qt (mg/g) rises with increasing contact time at all initial dye concentrations (Foo & Hameed, 2011a; Purkait et al., 2007; Sen et al., 2011). This is due to the fact that the initial dye concentration works as a driving force in overcoming dye mass transfer barrier between the aqueous and solid phases.

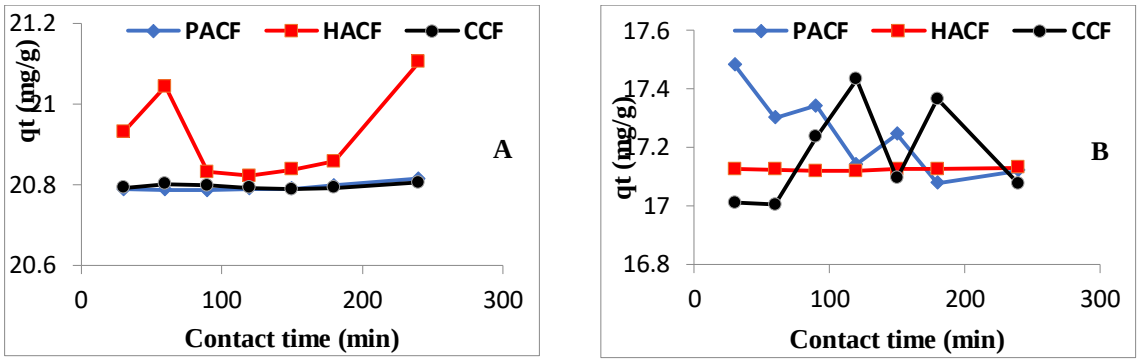

Figure 18: The effect of contact time (0.2 g of PACF, HACF and CCF) dosage on (A) methylene blue and (B) Congo red (20 ppm) adsorption. (Volume of dye: 50 ml; temperature 27 °C; agitation speed: 150 rpm)

3.2.3 Initial dye concentration

The initial dye concentration has significantly impacts the degree of dye removal. The effect of initial dye concentration is determined by the instantaneous interaction between dye concentration and accessible sites on an adsorbent surface. To evaluate the influence of initial dye concentrations, we prepared an adsorbent–adsorbate solution with a fixed adsorbent dose and varied initial dye concentrations at different time intervals and shake until equilibrium (Salleh et al., 2011).

Generally, when the initial dye concentration rises, the proportion of dye removed decreases, which could be due to the adsorption sites' saturation on the adsorbent surface. There will be vacant active sites on the adsorbent surface at low concentrations. As the initial dye concentration rises, the number of active sites necessary for dye molecule adsorption rises (Kannan & Sundaram, 2001). Increases in initial dye concentration, on the other hand, result in an increase in adsorbent capacity, which a stronger driving force could explain for mass transfer at higher initial dye concentrations (Bulut & Aydn, 2006).

At various initial dye concentrations, the effect of contact duration on Congo red dye adsorption onto *C. fistula* adsorbent was examined. The findings are shown in Fig. 19. The amount of dye adsorption rose from 4.66 mg/g to 19.18 mg/g for PACF, 3.18mg/g to 28.49 mg/g for HACF and 4.19 mg/g to 22.56 mg/g as the initial concentration of CR dye was increased from 20 ppm to 100 ppm. At all initial dye concentrations of CR, the adsorption capacity qt (mg/g) of adsorbent increases with increasing contact time, and equilibrium is reached within 240 min. However, adsorption of MB rose from 4.43 mg/g to 22.20 mg/g for PACF, 4.63 mg/g to 22.46 mg/g for HACF and 4.22 to 20.69 mg/g for CCF with highest percentage removal of 88.79, 89.83 and 82.77%, respectively.

Increasing the initial dye concentration provides the necessary driving power to overcome the resistance to mass dye transfer between the aqueous and solid phases explains these observations (Dawood, 2014). When using a constant dosage of adsorbent, the available adsorption active sites of the adsorbent become saturated at increasing initial dye concentrations, lowering the dye removal percentage of CR (Shahryari et al., 2010). The interaction between adsorbent and dye is also improved by increasing the starting concentration. As a result, increasing the initial dye concentration increases qt (mg/g) adsorption capacity.

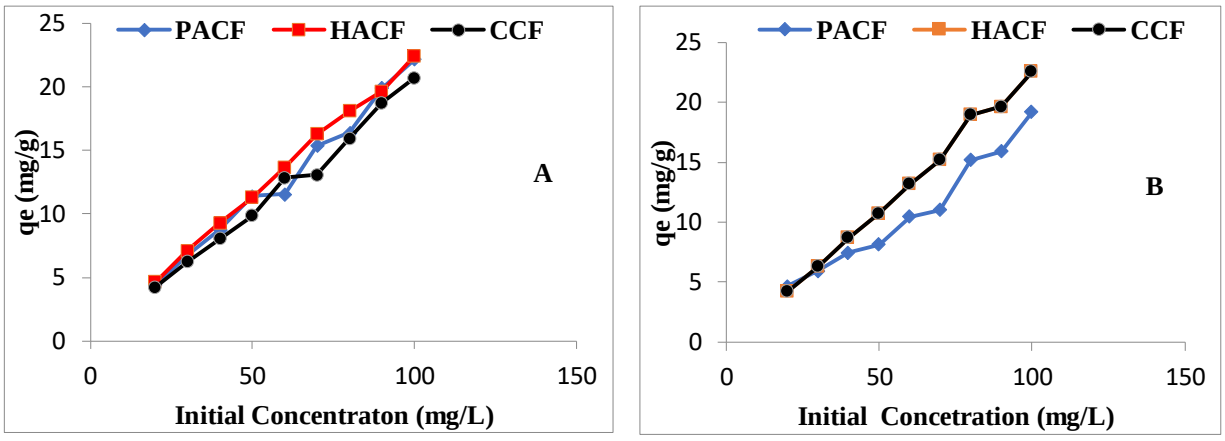

Figure 19: The effect of initial concentration (0.2 g of PACF, HACF and CCF) on (A) methylene blue and (B) Congo red adsorption

3.2.4 Effect of pH

Methylene blue (MB) is a cationic dye, strongly acidic at pH 2 and 3.5. Cationic dye adsorption is favored at pH > pHpzc. Therefore, pHpzc of the adsorption of MB onto *Cassia fistula* was at pH 9 (4.65 mg/g) for CCF, pH 10 (4.64 mg/g) for PACF and pH 11 (4.57 mg/g) for HACF. In another word, pH > pHpzc, a similar observation was reported by Yagub (2014), and Han et al. (2012).

However, Congo red (CR) is an anionic diazo dye. Anionic dyes are dyes with components that can make the dye molecule dissociate into negatively charged ions in an aqueous solution. Its color turns dark blue at acidic pH and red at alkaline pH, although the red color at neutral pH is slightly different from the original red color (Dawood, 2014). Anionic dye is favored at pH > pH_{pzc} where the surface becomes positively charged (Han et al., 2012). Maximum adsorption capacity of CR on to *Cassia fistula* was pH 5 (4.17 mg/g) for CCF, pH 5 (3.01 mg/g) for PACF and pH 3 (6.82 mg/g) HACF. This is due to the increase in proton densities and surface area of the adsorbent. Figure 20 shows the effect of pH variation on the adsorption of methylene blue and Congo red using the three adsorbents, respectively.

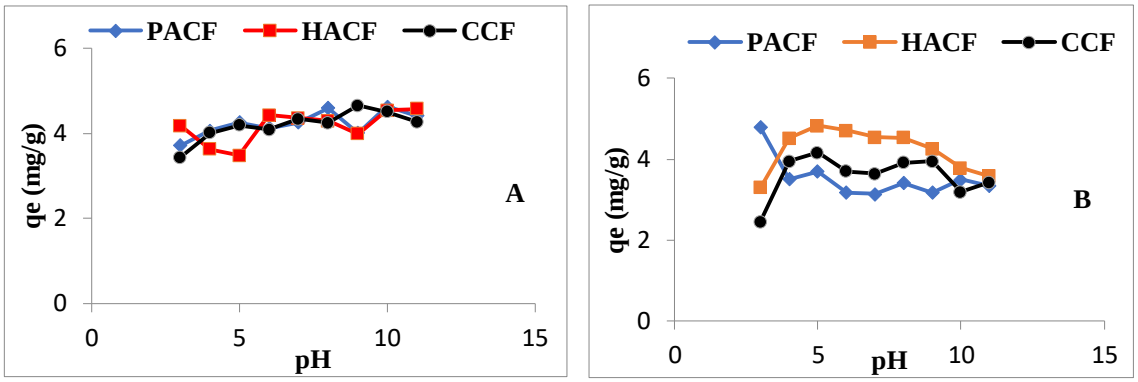

Figure 20: The Effect of pH (0.2g of PACF, HACF and CCF) Dosage on (A) Methylene blue and (B) Congo red (20ppm) adsorption.

3.2.5 Effect of temperature and thermodynamic studies

Figure 21 reveals the effect of temperature variation on the adsorption of methylene blue and Congo red, respectively. Temperature is a crucial parameter for the real application of MB and CR dye adsorption by C. fistula since some textile dye effluents are produced at quite high temperatures.

Adsorption is an endothermic process if the amount of adsorption increases as the temperature rises. This could be due to the dye molecules becoming more mobile and the number of active sites for adsorption increasing as the temperature rises. This impact is mostly determined by the mobility of dye molecules inside each dye. When the temperature rises, the adsorption capacity decreases, indicating that adsorption is an exothermic process. This could be caused by increasing temperatures, which reduce the adsorptive forces between dye species and active sites on the adsorbent surface, lowering adsorption quantity (Salleh et al., 2011).

As shown in Fig. 21, the amount of methylene blue adsorption on CCF, PACF and HACF rose as the temperature of the solution increased, indicating that the reaction was endothermic. A significant number of molecules may attain adequate energy to interact with active points on the surface. A similar result was also reported by Oladele et al. (2019) on the effect of temperature on unmodified and modified *C. fistula*.

To determine if an adsorption process is favorable or not, a thermodynamic analysis is required. The thermodynamic parameters free energy change (ΔG°), enthalpy change (ΔH°), and entropy change (ΔS°) all play a role in determining heat change in the dye and adsorbent adsorption process. The experimental research at different temperatures 300K, 303K, 308K, 313K, 318K, 323K, and 333K yielded Gibbs free energy change ΔG°,

enthalpy change ΔH°, and entropy change ΔS° using Eqs. 4 and 5 (Foo & Hameed, 2012) and the Van't Hoff plot (Fig. 22). Table 4 contains the list of all thermodynamic parameters.

The value of ΔG° increases, indicating that as the temperature increases, the adsorption of MB and CR on *Cassia fistula* biomass becomes more favorable. The positive value of ΔH° implies that the sorption process is endothermic and that the reaction consumes energy. In contrast, positive value of ΔS° shows that the solid-solute interface during adsorption is more random.

The adsorption capacities of PACF, HACF and CCF increased with increasing temperature on MB and CR at different temperatures.

$$\Delta G = -RTInK_{dc}\ S^{o} \quad (4)$$

$$Ink_{dc} = \frac{\Delta S^{o}}{R} - \frac{\Delta H^{o}}{R} \cdot \frac{1}{T} \quad (5)$$

Table 3: Thermodynamic parameters for removal of Congo red and methylene blue at different temperatures

	Temperature, T (K)	Congo red				Methylene blue			
		ΔG° ($kJmol^{-1}$)	ΔH° ($kJmol^{-1}$)	ΔS° ($kJ^{-1}mol^{-1}$)	R^2	ΔG° ($kJmol^{-1}$)	ΔH° ($kJmol^{-1}$)	ΔS° ($kJ^{-1}mol^{-1}$)	R^2
PACF	300	−0.0490	0.0030	0.7634	0.672	−0.0000	0.0019	20.0566	0.586
	303	−0.0545				−0.0245			
	308	−0.0633				−0.0271			
	313	−0.0720				−0.0324			
	318	−0.0862				−0.0370			
	323	−0.0960				−0.0495			
	333	−0.1194				−0.0562			
HACF	300	−0.0188	0.0007	0.6990	0.699	−0.0692	0.0001	0.3856	0.550
	303	−0.0209				−0.0770			
	308	−0.0243				−0.0892			
	313	−0.0278				−0.1027			
	318	−0.0313				−0.1160			
	323	−0.0348				−0.1291			
	333	−0.0419				−0.1566			
CCF	300	−0.0199	0.0024	3. 834	0.712	−0.0269	0.0005	1.0106	0.647
	303	−0.0226				−0.0299			
	308	−0.0264				−0.0349			
	313	−0.0303				−0.0399			
	318	−0.0343				−0.0459			
	323	−0.0383				−0.0500			
	333	−0.0483				−0.0605			

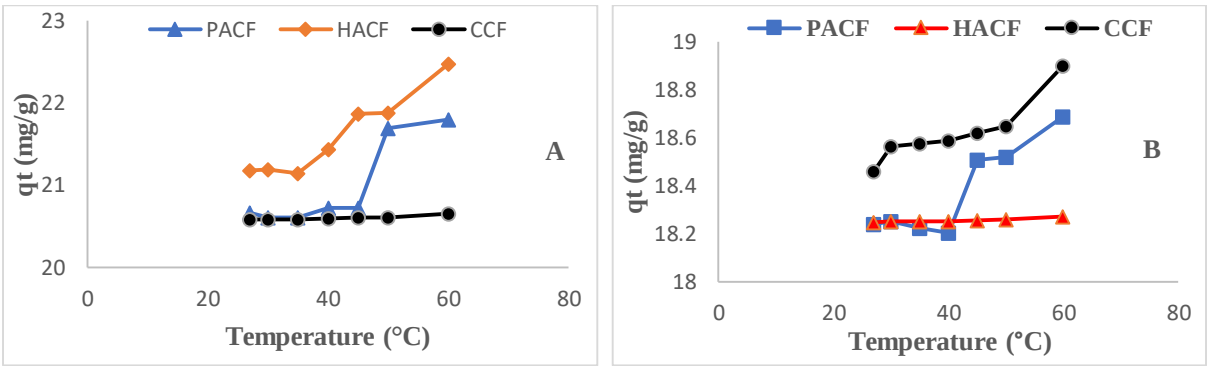

Figure 21: The effect of temperature (0.2g of PACF, HACF and CCF) on (A) methylene blue and (B) Congo red (100ppm) adsorption.

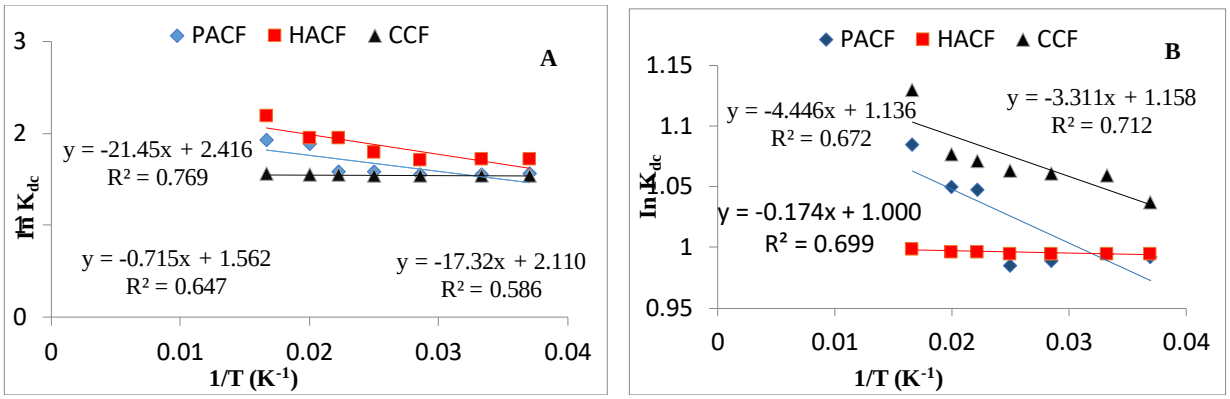

Figure 22: Van't Hoff plot for adsorption of (A) methylene blue and (B) Congo red on PACF, HACF and CCF

3.3 Adsorption equilibrium isotherms

Equilibrium isotherm experiments are critical for understanding how the MB and CR dye molecules interact with the *C. fistula* biomass surface and determining the adsorbent's maximum adsorption capacity. The applicability of the isotherm equation is assessed using correlation coefficients (R^2). The adsorbent could have a monolayer or multilayer surface. The fitting of isotherm data to various isotherm models is a crucial step in determining which model is best for design (El-Guendi, 1991). Langmuir, Freundlich, and Temkin isotherms were used to fit the data. The linear equation that represents the Langmuir isotherm (Langmuir, 1918) is as follows:

$$q_e = \frac{q_m K_{LC_e}}{1 + K_{LC_e}} \tag{6}$$

The linearized form of equation (6) is:

$$\frac{Ce}{qe} = \frac{1}{K_{Lqe}} + \frac{Ce}{qm} \tag{7}$$

Where Ce denotes the equilibrium concentration in mg/L, qe denotes the quantity of adsorbate ion sorbed in mg/g, and qm denotes the qe for a full monolayer in mg/g. The adsorption energy KL (L/mg) determines the Langmuir constant. When Ce/qe against Ce is plotted, a straight line appears (Fig. 23). Table 5 lists the Langmuir constants derived from this isotherm. The separation factor (RL) is a dimensionless parameter that can be

determined using Equation 8 (Langmuir, 1918) to determine the feasibility of an adsorption system at various initial dye concentrations:

$$R_L = \frac{1}{1+(K_{LC_O})} \quad (8)$$

The initial dye concentration is defined as C_o (mg/L). The kind of isotherm is determined by the value of R_L, which might be unfavorable ($R_L > 1$), linear ($R_L = 1$), favorable ($0 < R_L < 1$), or irreversible ($R_L = 0$) (Kaur et al, 2013). Values of R_L for PACF, HACF and CCF were found to be 0.2045, 3.762×10^{-3} and 0.0164, respectively for methylene blue and 6.106×10^{-3}, 1.00 and 0.0413, respectively for Congo red confirmed that the adsorbent is favorable for adsorption of MB and CR dye under conditions studied. The correlation coefficients (R^2) show that Langmuir isotherm is not applicable to this adsorption study.

Table 4: Isotherm parameters for MB and CR adsorption

Isotherms	Parameters	Adsorbents					
		Methylene blue			Congo red		
		PACF	HACF	CCF	PACF	HACF	CCF
Langmuir	$q_{m\ (mg/g)}$	22.198	22.4586	20.6926	19.1802	17. 8769	22.5600
	K_L (L/mg)	0.039	2.648	0.5989	1.6276	-3.219×10^{-3}	-0.2519
	R^2	0.517	0.798	0.279	0.543	0.008	0.015
	R_L	0.2045	3.762×10^{-3}	0.0164	6.106×10^{-3}	1.00	0.0413
Freundlich	K_f (mg/L)	4.4952	0.450	1.6905	3.443	0.3482	1.9719
	n	1.497	0.9042	1.225	1.0406	0.9615	1.0406
	1/n	0.668	1.106	0.816	0.415	1.040	0.9042
	R^2	0.918	0.742	0.878	0.708	0.666	0.527
Temkin	K_T (mg/L)	3406.13	0.894	0.940	1000.696	1.085×10^{12}	1.133×10^{12}
	b_T (KJ/mol)	27.714	21.14	26.53	17.56	4. 815	55.43
	R^2	0.645	0.910	0.765	0.536	0.518	0.455

The linearised format of Freundlich isotherm model (Freundlich, 1906):

$$\ln q_e = \frac{1}{n} \ln C_e + \ln K_f \quad (9)$$

Where C_e is the equilibrium concentration of dye in solution (mg/L) and q_e (mg/g) is the amount of dye adsorbed at equilibrium time. From the slope and intercept of the linear plot of $\ln q_e$ against $\ln C_e$, the system's adsorption capacity, K_f, and the heterogeneity factor, 1/n, can be estimated. The other Freundlich constant, n, is a measurement of the adsorption's divergence from linearity and is used to test adsorption types. If n equals unity (1), the adsorption should be linear, according to the theory. Furthermore, adsorption is a chemical process when n is less than one, and a favorable adsorption is a physical process when n is greater than one (1) (Salleh et al., 2011; Sen et al., 2011; Vimonses et al., 2009).

The plot of ln q_e against ln C_e (Fig. 24) gives straight lines with a slope of 1/n. The adsorption of MB and CR follows the Freundlich isotherm, as seen in Fig. 5. Freundlich constants (K_f and n) were determined as a result and are listed in Table 5. Table 5 further reveals that for MB and CR adsorption on PACF, HACF, and CCF, high regression values were reached. As a result, the adsorption equilibrium data fits the Freundlich isotherm model and adsorption process well. The value of 'n' is greater than 1 (near unity), indicating that adsorption is a favourable physical process.

Temkin isotherm (Temkin and Pyzhev, 1940) is represented by the following Equation 10:

$$q_e = \frac{RT}{b}(\ln K_t C_e) \quad (10)$$

Equation 7 can be expressed in its linear form as:

$$q_e = B_T \ln KT + B_T \ln C_e \quad (11)$$

$$\text{Where } B_T = \frac{RT}{b} \quad (12)$$

Where T (K) is absolute temperature, while R is the universal gas constant (8.314 J/ (mol^{-1}K)). The equilibrium binding energy and the heat of adsorption were represented by the Temkin constants K_T (L/mg) and B_T. The slope and intercept of the linear equation of the plot where q_e against lnC_e can be used to determine these constants (Fig. 25). The values of the parameters are given in Table 5.

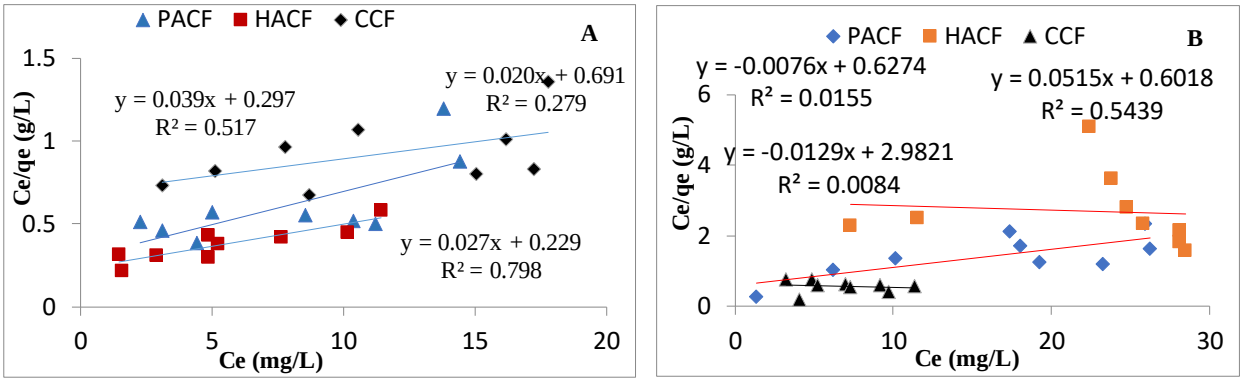

Figure 23: Linearized Langmuir adsorption isotherm of (A) MB and (B) CR on PACF, HACF and CCF

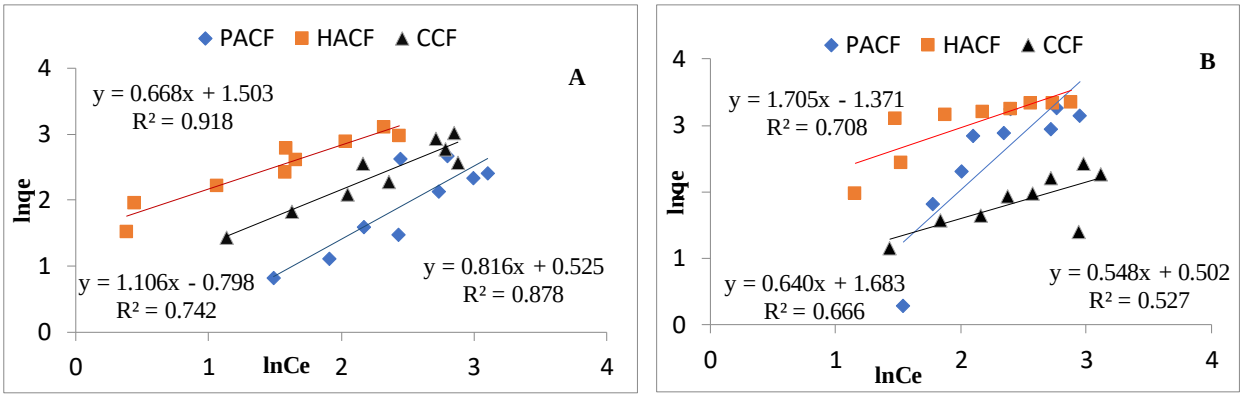

Figure 24: Linearized Freundlich adsorption isotherm of (A) MB and (B) CR on PACF, HACF and CCF

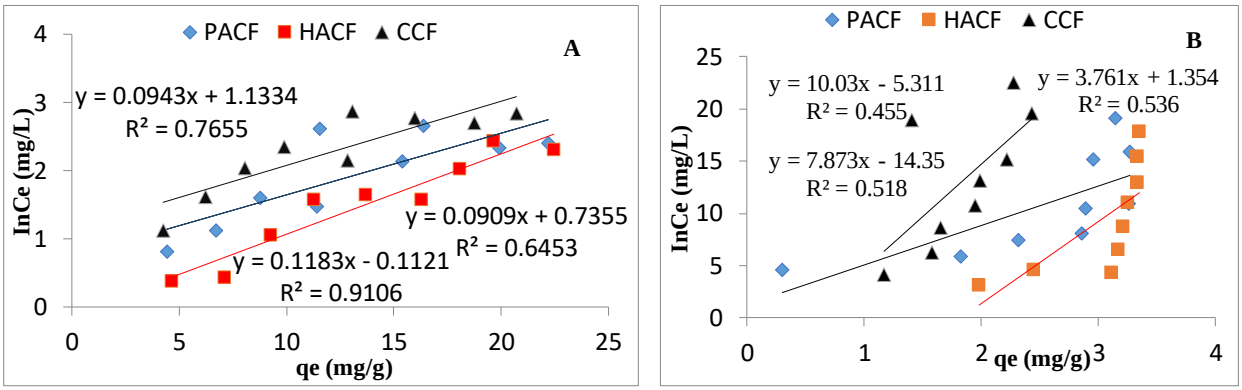

Figure 25: Linearized Temkin adsorption isotherm of (A) MB and (B) on PACF, HACF and CCF

3.4 Adsorption kinetics

Kinetic models are determined using chemical reaction or diffusion mass transfer control through adsorption process controlling mechanisms. To establish the optimal operating conditions for the full-scale batch operation, the kinetics of dye adsorption onto adsorbent materials are required. The study of adsorption kinetics demonstrates the solute uptake rate, which determines the adsorbate's residence time at the solution interface. When building an adsorption system, this rate is critical, and may be estimated via a kinetic study.

The design of an industrial adsorption system relies heavily on the prediction of batch adsorption kinetics. The physical and chemical features of the adsorbent system and the system circumstances will determine the nature of the adsorption process.

Lagergren's pseudo-first-order rate expression (Liu et al., 2019) is used to determine the adsorption rate constant:

$$\log (q_e - q_t) = \log q_e \frac{k_1}{2.30003} t \quad (13)$$

Where qt and qe are the amounts of adsorbate adsorbed (mg g^{-1}) at a certain time, t (min), and at equilibrium, respectively; k_1 is the pseudo-first-order adsorption rate constant (min^{-1}) and t is the contact duration (min). In Table 5, the slope and intercept of a linear plot of log ($q_e - q_t$) versus t (Fig. 26) yielded the values of k_1 and q_e, respectively. The use of the first-order kinetics model is indicated by a straight line of log ($q_e - q_t$) versus t. log q_e should be equal to the intercept of the plot of log ($q_e - q_t$) against t in a true first-order process. Lagergren pseudo-first-order model gave a poor linear regression coefficient (R^2) of less than 0.624 at various physico-chemical conditions as shown in Table 5 to evaluate the kinetics of the adsorption of CR and MB on CCF, PACF, and HACF. The pseudo-second-order model (Ho & McKay, 1999) was used to analyze further the kinetic data, which was expressed as:

$$\frac{t}{qt} = \frac{1}{k2q2e} + \frac{1}{qe} t \quad (14)$$

The pseudo-second-order adsorption rate constant k_2 (g mg^{-1} min^{-1}) is used here. The rate constant k_2 (g mg^{-1} min^{-1}), initial sorption rate h (mg g^{-1} min^{-1}), and q_e (mg g) may all be estimated from a plot of t/q_t vs. t. For the applicability of the second-order kinetic, a plot of t/qt vs t should yield a linear relationship.
The initial sorption rate h, at time $t \rightarrow 0$, is calculated using the constant k_2 as presented in Equation 15 (Ho & McKay, 1999):

$$h = k_2 q_e \quad (15)$$

Thus, the plot of t/qt may be used to calculate the constant rate k_2, initial adsorption rate h, and predicted qe. Time t using pseudo-second-order. With an $R^2 \geq 0.999$, the model matches the kinetic data better than pseudo-first-order kinetic models (Table 5). These findings imply that the pseudo-second-order kinetic model with high correlation coefficients best describes the adsorption of MB and CR on PACF, HACF, and CCF (Fig. 27).

However, Largitte and Pasquier (2016) described the Elovich model as follows:

$$q_t = \frac{1}{\beta} \text{In} (\alpha\beta t) \quad (16)$$

Where α is the Elovich model's initial adsorption rate (mg/g), and β is the constant related to surface coverage and chemisorption activation energy (g/mg). The plot presented in Figure 28 reveals that the adsorbents do not give good plots when their kinetic data is fitted for practicability.

3.5 Intraparticle diffusion

The Weber & Moris (1963) model was used to study the intraparticle diffusion mechanism. The model is described in Equation 17.

$$q_t = K_{id} t^{0.5} + C \quad (17)$$

Where qt is the adsorption capacity at time t, $t^{0.5}$ is the half-life in seconds, K_{id} (mg g^{-1} $min^{-0.5}$) is the intraparticle diffusion rate constant, and C (mg g^{-1}) is a constant that gives an idea of boundary layer thickness. Plotting qt vs. $t^{0.5}$ gives a linear relationship where K_{id} can be calculated from the slope (Fig. 29). Intraparticle diffusion is the rate-determining step if the plot passes through the origin. However, the linear plots (Fig. 29) did not pass through the origin for each concentration. This suggests that intraparticle diffusion was not a rate-controlling process.

Table 5: Kinetic parameters for the adsorption of methylene blue and Congo red on the adsorbents

Kinetic Parameters	Methylene blue			Congo Red		
q_e experimental (mg/g)	20.8142	21.104	20.8047	17.4817	17.1308	17.4337
			Pseudo-first-order Kinetic			
	PACF	HACF	CCF	PACF	HACF	CCF
q_e calculated (mg/g)	8.897×10^{-3}	0.0800	1.773×10^{-3}	0.3434	0.1877	0.476
k_1 (min^{-1})	0.012	0.009	0.019	0.000	0.000	0.003
R^2	0.402	0.624	0.599	0.007	0.283	0.086
			Pseudo-second-order Kinetic			
q_e calculated (mg/g)	20.833	0.0475	0.0481	0.0587	0.0584	17.241
h (mg/g/min)	9.5911	−13774.6	−1.602	5,1092.54	1.000	−4.1840
K_2 (g/mg/min)	0.4608	−652.7	−0.077	2,922.63	−6818. 8	−0.240
R^2	1	0.999	1	1	1	0.999
			Elovich Kinetic			
β	111.11	500	1000	83.33	1000	9.524
R^2	0.468	0.000	0.021	0.028	0.082	0.187
			Intra-particle diffusion Kinetic			
Kd (g/mg/min)	0.002	0.003	0.000	−0.036	0.000	0.018
C (mg/g)	20.76	20.88	20.79	17.63	17.11	16.98
R^2	0.611	0.011	0.033	0.781	0.172	0.128

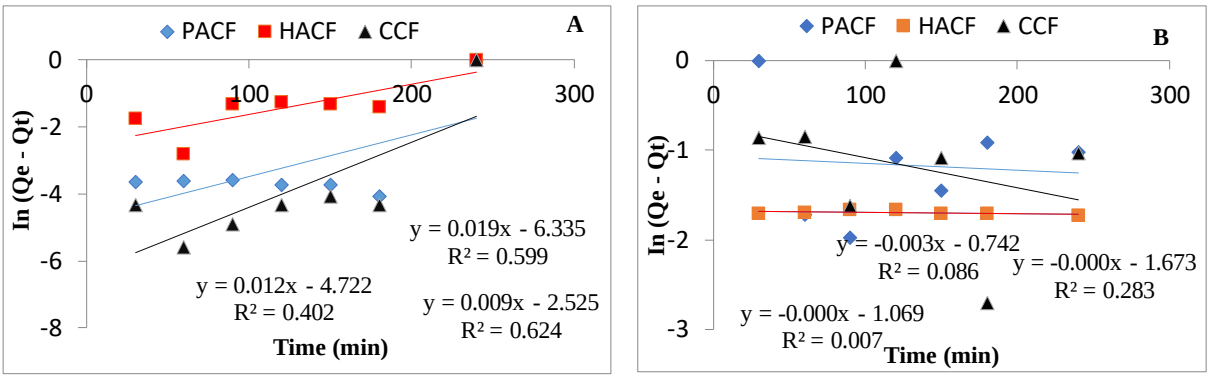

Figure 26: Pseudo-first-order kinetics for adsorption of (A) MB and (B) CR adsorption onto PACF, HACF and CCF

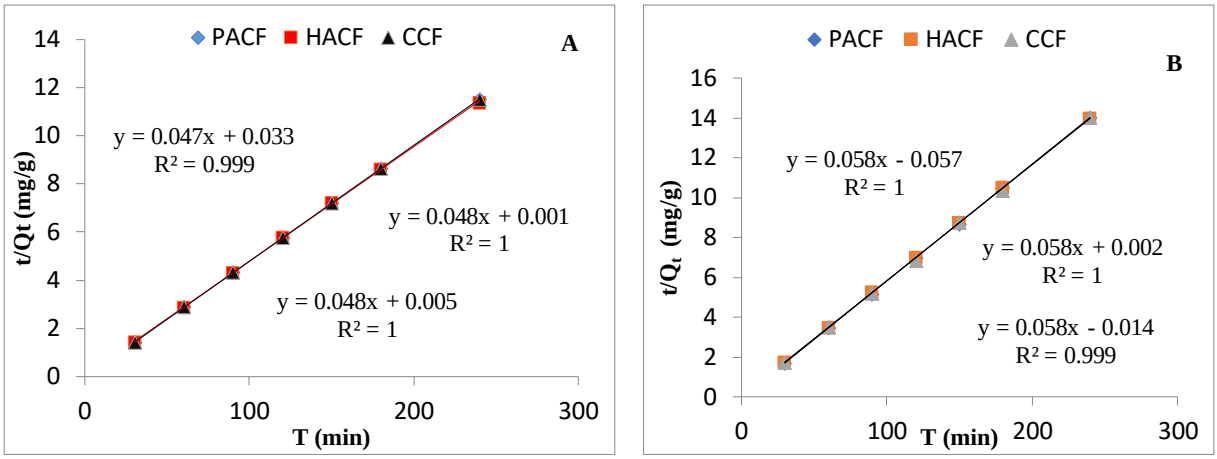

Figure 27: Pseudo-second-order kinetics for adsorption of (A) MB and (B) CR adsorption onto PACF, HACF and CCF

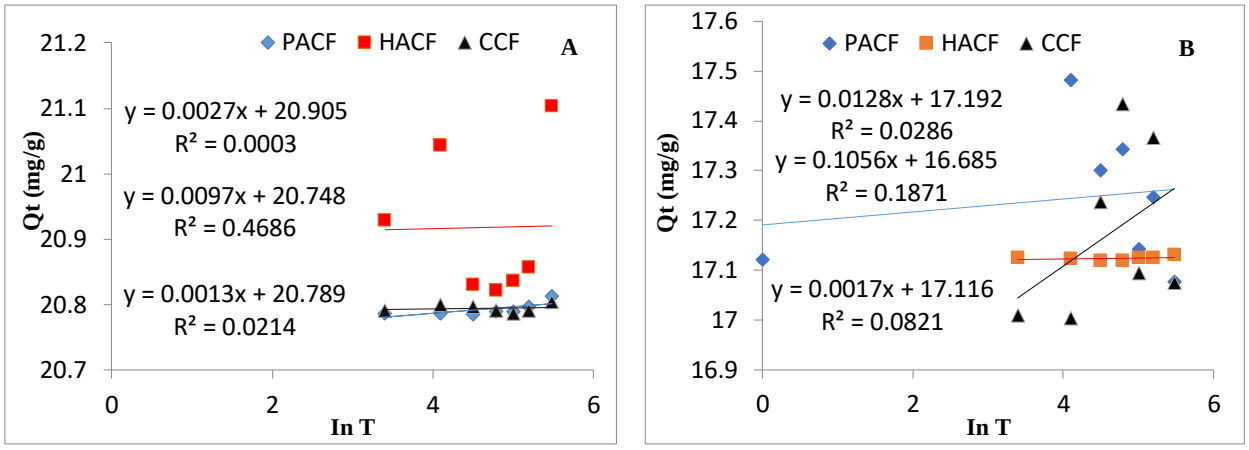

Figure 28: Elovich kinetics for adsorption of (A) MB and (B) adsorption onto PACF, HACF and CCF

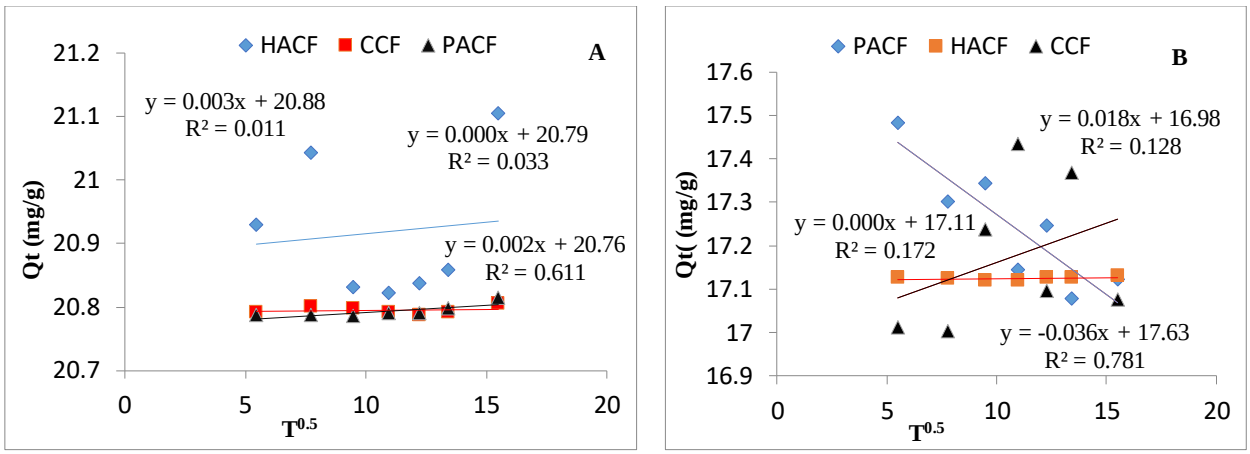

Figure 29: Intra-Particle kinetics for adsorption of (A) MB and (B) CR adsorption onto PACF, HACF and CCF

4. Conclusion

This research examined the effectiveness of biomass of carbonized *Cassia fistula* (CCF), potassium hydroxide activated *Cassia fistula* (PACF), and hydrogen peroxide activated *Cassia fistula* (HACF) pods for removing methylene blue (MB) and Congo red (CR) from aqueous solution and the following are the findings:

i. The amount of methylene blue and Congo red dye uptake on carbonized and chemically activated *Cassia fistula* biomass was found to increase with a decrease dosage; increase with increase in solution pH; increase with the increase in initial dye concentration; increase with the increase in contact time; increase with the increase in system temperature for PACF, HACF, and CCF.
ii. The kinetic experiments in the batch research showed that dye adsorption was rapid initially, followed by a slower phase where equilibrium uptake was reached.
iii. Methylene blue and Congo red adsorption followed pseudo-second-order kinetics models, according to the kinetic studies.
iv. Within this initial dye concentration range of 100 ppm, the Freundlich equation can describe the adsorption of methylene blue and Congo red on carbonized and chemically activated *Cassia fistula* biomass. PACF's maximum heterogeneous adsorption capacity was 20.81 mg/g at pH 10.0. In contrast, HACF's maximum heterogeneous adsorption capacity was 21.10 mg/g at pH 11.0 and CCF was 20.80 mg/g at pH 9.0 for methylene blue and 4.17 mg/g at pH 5 for CCF, 3.01 mg/g at pH 5 for PACF and 6.82 mg/g at pH 3 HACF for Congo red at the same experimental conditions.
v. The Freundlich constant, n, indicates favorable adsorption and a physical process.
vi. According to the thermodynamic study, the system is spontaneous, endothermic, and physical.
vii. Overall, these experimental and theoretical results provided new insights into the dye adsorption mechanism.

Conflict of interests

The authors have not disclosed any conflicts of interest in relation to this work.

References

Afroze, S., Sen, T. K. & Ang, M. (2015). Agricultural Solid Wastes in Aqueous Phase Dye Adsorption: A Review. In: Foster, C. (Ed), *Agricultural Wastes: Characteristics, Types and Management*, pp. 169-213. USA: Nova Publishers.

Afroze, S., & Sen, T.K. (2018). A review on heavy metal ions and dye adsorption from water by agricultural solid waste adsorbents. *Water, Air, & Soil Pollution*, 229, 225. https://doi.org/10.1007/s11270-018-3869-z

Bensalah, N., Alfaro, M., & Martínez-Huitle, C. (2009). Electrochemical treatment of synthetic wastewaters containing Alphazurine A dye. *Chemical Engineering Journal*, 149, 348–352. https://doi.org/10.1016/j.cej.2008.11.031

Bhat, R. V. & Mathur, P. (1998). Changing scenario of food colours in India. *Current Science*, 74(3), 198–202.

Bulut, Y. & Aydin, H. (2006). Kinetics and thermodynamics study of methylene blue adsorption on wheat shells. *Desalination*, 194, 259–267. https://doi.org/10.1016/j.desal.2005.10.032

Carmen, Z. & Daniela, S. (2012). Textile Organic Dyes – Characteristics, Polluting Effects and Separation/Elimination Procedures from Industrial Effluents – A Critical Overview. In: Puzyn, T. & Mostrag-Szlichtyng, A. (Eds.), *Organic Pollutants Ten Years After the Stockholm Convention - Environmental and Analytical Update* (pp. 55-86). Rijeka, Croatia: IntechOpen. https://doi.org/10.5772/32373

Crini, G. (2006). Non-conventional low-cost adsorbents for dye removal: a review. *Bioresource Technology*, 97(9), 1061– 1085. https://doi.org/10.1016/j.biortech.2005.05.001

Cook, S. M. F. & Linden, D. R. (1997). Use of Rhodamine WT to facilitate dilution and analysis of Atrazine samples in short-term transport studies. *Journal of Environmental Quality*, 26(5), 1438-1440. https://doi.org/10.2134/jeq1997.00472425002600050035x

Dawood, S. Sen, T.K. & Phan, C. (2014). Synthesis and characterisation of novel-activated carbon from waste biomass Pine Cone and its application in the removal of Congo red dye from aqueous solution by adsorption. *Water, Air, & Soil Pollution*, 225, 1818. https://doi.org/10.1007/s11270-013-1818-4

Demirbas, A. (2009). Agricultural based activated carbons for the removal of dyes from aqueous solutions: a review. *Journal of Hazardous Materials,* 167(1-3), 1–9. https://doi.org/10.1016/j.jhazmat.2008.12.114

Dickhout, J.M., Moreno, J., Biesheuvel, P.M., Boels, L., Lammertink, R.G.H. & de Vos, W.M. (2017). Produced water treatment by membranes: a review from a colloidal perspective. *Journal Colloid Interface Science,* 487, 523−534. https://doi.org/10.1016/j.jcis.2016.10.013

El-Geundi, M. S. & Nassar, M. M. (1991). Comparative cost of colour removal from textile effluents using natural adsorbents. *Journal of Chemical Technology and Biotechnology*, 50(2), 257-264. https://doi.org/10.1002/jctb.280500210

Feng, Y., Zhou, H., Liu, G., Qiao, J., Wang, J., Liu, H., Yang, L. & Wu, Y. (2012). Methylene blue adsorption onto swede rape straw (*Brassica napus* L.) modified by tartaric acid: Equilibrium, kinetic and adsorption mechanisms. *Bioresource Technology,* 125, 138-144. https://doi.org/10.1016/j.biortech.2012.08.128

Freundlich, H. (1906). Over the adsorption in solution. *Journal of Physical Chemistry,* 57, 385–470.

Foo, K.Y. & Hameed, B.H. (2012). Microwave-assisted preparation and adsorption performance of activated carbon from biodiesel industry solid reside: influence of operational parameters. *Bioresource Technology,* 103 (1), 398−404. https://doi.org/10.1016/j.biortech.2011.09.116

Gibson N., Kuchenbecker, P., Rasmussen K., Hodoroaba V. D. & Rauscher H. (2020). Volume-specific Surface Area by Gas Adsorption Analysis with the BET Method. In: Hodoroaba, V-D., Unger, W.E.S. and Shard, A.G., *Characterization of* Nanoparticles (pp. 265-294). Amsterdam, Netherlands: Elsevier. https://doi.org/10.1016/B978-0-12-814182-3.00017-1

Han, R., Wang, Y., Han, P., Shi, J., Yang, J. & Lu, Y. (2006). Removal of methylene blue from aqueous solution by chaff in batch mode. *Journal of Hazardous Materials,* 137, 550–557. https://doi.org/10.1016/j.jhazmat.2006.02.029

Ho, Y.-S. & McKay, G. (1999). Pseudo-second order model for sorption processes. *Process Biochemistry,* 34 (5), 451–465. https://doi.org/10.1016/S0032-9592(98)00112-5

Imran, M., Suddique, M., Shah, M.G., Ahmad, I., Murtaza, B., Shah, N.S., Mubeen, M., S. Ahmad, S., Zakir, A. & Schotting, R. J. (2019). Kinetic and equilibrium studies for cadmium biosorption from contaminated water using *Cassia fistula* biomass. *International Journal Environmental Science and Technology,* 16, 3099–3108. https://doi.org/10.1007/s13762-018-1872-y.

Jadhav, J., Kalyani, D., Telke, A., Phugare, S. & Govindwar, S. (2010). Evaluation of the efficacy of a bacterial consortium for the removal of color, reduction of heavy metals, and toxicity from textile dye effluent. *Bioresource Technology*, 101(1), 165–173. https://doi.org/10.1016/j.biortech.2009.08.027

Kabdaşli, I., Tünay, O., & Orhon, D. (1999). Wastewater control and management in a leather tanning district. *Water Science and Technology*, 40(1), 261–267. https://doi.org/10.1016/S0273-1223(99)00393-5

Kannan, N. & Sundaram, M. M. (2001). Kinetics and mechanism of removal of methylene blue by adsorption on various carbons—a comparative study. *Dyes and Pigments*, 51(1), 25-40. https://doi.org/10.1016/S0143-7208(01)00056-0

Kaur, S., Rani, S. & Mahajan, R.K. (2013). Adsorption kinetics for the removal of hazardous dye Congo red by biowaste materials as adsorbents. *Journal of Chemistry,* 2013, 628582. https://doi.org/10.1155/2013/628582

Kross, B. C., Nicholson, H. F. & Ogilvie, L. K. (1996). Methods development study for measuring pesticide exposure to golf course workers using video imaging techniques. *Applied Occupational and Environmental Hygiene,* 11(11), 1346– 1350. https://doi.org/10.1080/1047322X.1996.10389423

Langmuir, I. (1918). The adsorption of gases on plane surfaces of glass, mica and platinum. *Journal of the American Chemical Society*, 40(9), 1361–1403. https://doi.org/10.1021/ja02242a004

Largitte, L. & Pasquier, R. (2016). A review of the kinetics adsorption models and their application to the adsorption of lead by an activated carbon. *Chemical Engineering Research and Design,* 109, 495-504. https://doi.org/10.1016/j.cherd.2016.02.006

Liu, L., Li, Y. & Fan, S. (2019). Preparation of KOH and H_3PO_4 modified biochar and its application in methylene blue removal from aqueous solution. *Processes*, 7(12), 891. https://doi.org/10.3390/pr7120891

Matulik, A.G., Kerstetter, D.W., Hammerschlag, N., Divoll, T., Hammerschmidt, C.R. & Evers, D.C. (2017). Bioaccumulation and biomagnification of mercury and methylmercury in four sympatric coastal sharks in a protected subtropical lagoon. *Marine Pollution Bulletin*, 116(1−2), 357−364. https://doi.org/10.1016/j.marpolbul.2017.01.033

Moreira, F.C., Boaventura, R.A.R., Brillas, E. & Vilar, V.J.P. (2017). Electrochemical advanced oxidation processes: a review on their application to synthetic and real wastewaters. *Applied Catalysis B: Environmental*, 202, 217−261. https://doi.org/10.1016/j.apcatb.2016.08.037

Oladele, S. O., Adeyemo, A. J. & Awodun, M. A. (2019). Influence of rice husk biochar and inorganic fertilizer on soil nutrients availability and rain-fed rice yield in two contrasting soils. *Geoderma*, 336, 1-11. https://doi.org/10.1016/j.geoderma.2018.08.025

Purkait, M. K., Maiti, A. Gupta, S. D. & De, S. (2007). Removal of Congo red using activated carbon and its regeneration. *Journal of Hazardous Materials*, 145, 287-295. https://doi.org/10.1016/j.jhazmat.2006.11.021

Peng, C., Chai, L. Y., Tang, C. J., Min, X. B., Ali, M., Song, Y. X., & Qi, W. M. (2017). Feasibility and enhancement of copper and ammonia removal from wastewater using struvite formation: a comparative research. *Journal of Chemical Technology and Biotechnology*, 92(2), 325–333. https://doi.org/10.1002/jctb.5009

Polanco Rodriguez, A.G., Inmaculada Riba Lopez, M., Angel DelValls Casillas, T., Leon, J.A., Anjan Kumar Prusty, B. & Alvarez Cervera, F.J. (2017). Levels of persistent organic pollutants in breast milk of Maya women in Yucatan, Mexico. *Environmental Monitoring and Assessment,* 189(2), 59. https://doi.org/10.1007/s10661-017-5768-y

Schweiter, L. & Noblet, J. (2018). Water Contamination and Pollution. In: Török, B and Dransfield, T. (Eds), *Green Chemistry: An Inclusive Approach* (pp. 261-290). Amsterdam, Netherlands: Elsevier. https://doi.org/10.1016/B978-0-12-809270-5.00011-X

Shahryari, Z., Goharrizi, A. S., & Azadi, M. (2010). Experimental study of methylene blue adsorption from aqueous solutions onto carbon nano tubes. *International Journal of Water Resources Environmental Engineering.* 2(2), 16-28.

Sokolowska-Gajda, J., Freeman, H. S. & Reife, A. (1996). Synthetic dyes based on environmental considerations. Part 2: Iron complexes formazan dye. *Dyes and Pigments,* 30(1), 1-20. https://doi.org/10.1016/0143-7208(95)00048-8

Sari, A., Tuzen, M., Citak, D. & Soylak, M. (2007). Equilibrium, kinetic and thermodynamic studies of adsorption of Pb (II) from aqueous solution onto Turkish kaolinite clay. *Journal of Hazardous Materials*, 149(2), 283–291. https://doi.org/10.1016/j.jhazmat.2007.03.078

Salleh, M.A.M., Mahmoud, D.K., Karim, W.A. & Idris, A., (2011). Cationic and anionic dye adsorption by agricultural solid wastes: a comprehensive review. *Desalination*, 280, 1-13. https://doi.org/10.1016/j.desal.2011.07.019

Scarpi, C., Ninci, F., Centini, M., & Anselmi, C. (1998). High-performance liquid chromatography determination of direct and temporary dyes in natural hair colourings. *Journal of Chromatography A,* 796(2), 319–325. https://doi.org/10.1016/S0021-9673(97)01015-7

Sen, T. K., Afroze, S. & Ang, H. (2011). Equilibrium, kinetics and mechanism of removal of methylene blue from aqueous solution by adsorption onto pine cone biomass of *Pinus radiata*. *Water, Air, &Soil Pollution*, 218, 499–515. https://doi.org/10.1007/s11270-010-0663-y

Sohaimi, K.S.A., Ngadi, N., Mat, H., Inuwa, I.M. & Wong, S., (2017). Synthesis, characterization and application of textile sludge biochars for oil removal. *Journal of Environmental Chemical Engineering,* 5(2), 1415−1422. https://doi.org/10.1016/j.jece.2017.02.002

Tan, J., Zhang, X., Wei, X. & Wang, L. (2012). Removal of malachite green from aqueous solution using waste newspaper fiber. *Bioresources*, 7(3), 4307-4320.

Tatsuta, N., Murata, K., Iwai-Shimada, M., Yaginuma-Sakurai, K., Satoh, H. & Nakai, K. (2017). Psychomotor ability in children prenatally exposed to methylmercury: the 18-month follow-up of Tohoku study of child development. *The Tohoku Journal of Experimental Medicine*, 242 (1), 1−8. https://doi.org/10.1620/tjem.242.1

Tünay, O., Kabdaşli, I., Orhon, D. & Cansever, G. (1999). Use and minimization of water in leather tanning processes. *Water Science and Technology*, 40(1), 237–244. https://doi.org/10.1016/S0273-1223(99)00390-X

UN Water. (2017). UN World Water Development Report. unwater.org. (Accessed 30 September 2021).

UNESCO (2017). The Global Water Quality Challenge & SDGs. unesco.org. (Accessed 21 May, 2017)

Weber, W., and Morris, J. (1963). Kinetics of adsorption on carbon from solution. *Journal of the Sanitary Engineering Division*, 89(2), 31–60. https://doi.org/10.1061/JSEDAI.0000430

Wong, S., Lee, Y., Ngadi, N., Inuwa, I. M. &Mohamed, N.B. (2017). Synthesis of activated carbon from spent tea leaves for aspirin removal. *Chinese Journal of Chemical Engineering,* 26(5), 1003-1011. https://doi.org/10.1016/j.cjche.2017.11.004

Wróbel, D., Boguta, A., & Ion, R. M. (2001). Mixtures of synthetic organic dyes in a photoelectrochemical cell. *Journal of Photochemistry and Photobiology A: Chemistry*, 138(1), 7–22. https://doi.org/10.1016/S1010-6030(00)00377-4

Yagub, M. T., Sen, T. K., Afroze, S. & Ang, H. M. (2014). Dye and its removal from aqueous solution by adsorption: A review. *Advances in Colloid and Interface Science*, 209, 172-184. https://doi.org/10.1016/j.cis.2014.04.002

Ye, B.S., Leung, A.O.W. & Wong, M.H. (2017). The association of environmental toxicants and autism spectrum disorders in children. *Environmental Pollution*, 227, 234–242. https://doi.org/10.1016/j.envpol.2017.04.039

Yingwen, X., Bin, G., Ying, Y., Mandu, I., Ming, Z., Andrew R., Zimmerman, A. R. & Kyoung, S.R. (2012). Hydrogen peroxide modification enhances the ability of biochar (hydrochar) produced from hydrothermal carbonization of peanut hull to remove aqueous heavy metals: Batch and column tests. *Chemical Engineering Journal*, 200-202, 673-680. https://doi.org/10.1016/j.cej.2012.06.116

Zenker, A., Cicero, M.R., Prestinaci, F., Bottoni, P. & Carere, M. (2014). Bioaccumulation and biomagnification potential of pharmaceuticals with a focus to the aquatic environment. *Journal of Environmental Management*, 133, 378–387. https://doi.org/10.1016/j.jenvman.2013.12.017